

Chemotactic Feedback Controls Patterning in Hybrid Tumor–Stroma Model

Jiguang Yu^{1†}, Louis Shuo Wang^{2*†}, Zonghao Liu³, Jingfeng Liu^{3*}

¹College of Engineering, Boston University, Boston, 02215, MA, United States.

²Department of Mathematics, University of Tennessee, Knoxville, 37996, TN, United States.

³Department of Hepatopancreatobiliary Surgery, Fujian Cancer Hospital, Fuzhou, 350014, Fujian, China.

*Corresponding author(s). E-mail(s): swang116@vols.utk.edu;
drjingfeng@126.com;

Contributing authors: jyu678@bu.edu; liuzonghao@fjmu.edu.cn;

†These authors contributed equally to this work as co-first authors.

Abstract

Motivated by an ongoing collaboration with clinical oncologists and pathologists, we develop a hybrid partial differential equation–ordinary differential equation (PDE–ODE) framework that captures (i) competition between susceptible and resistant phenotypes, (ii) stromal state switching, and (iii) a clinically realistic open-loop, single-dose therapeutic agent \mathbf{I} with diffusion and clearance.

Clinical management of solid tumors is increasingly limited by spatial heterogeneity and therapy-induced resistance niches that are difficult to predict from well-mixed models. We establish a rigorous mathematical backbone with forward invariance of the nonnegative cone and global-in-time well-posedness. Exploiting the decoupled drug equation $\partial_t \mathbf{I} = \mathbf{d}_I \Delta \mathbf{I} - \gamma_I \mathbf{I}$, we prove a long-time reduction during washout and show that the damped base dynamics admit no diffusion-driven (Turing-type) instability. We then formulate a directionality–damping principle: unidirectional (open-loop) sensing yields at most transient focusing, whereas bidirectional (closed-loop) feedback reshapes the effective mobility and produces explicit thresholds separating stable homogeneity, finite-band patterning (resistance niche formation), and aggregation when strong parabolicity is violated. Reproducible simulations corroborate this classification and highlight when flux regularization is required for physical realism.

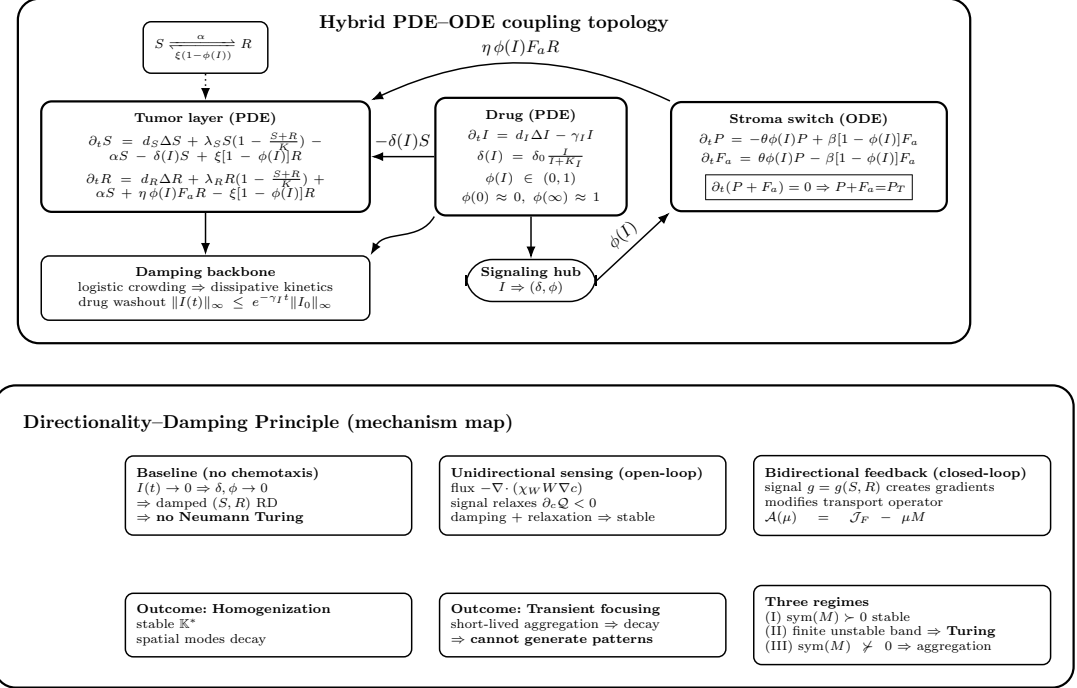


Fig. 1 Unified mechanism diagram. Top: hybrid PDE-ODE coupling topology for tumor phenotypes (S, R) , drug I , and stromal switching (P, F_a) under Neumann boundary conditions. Bottom: the directionality-damping principle: (i) drug washout and logistic damping enforce baseline homogenization (no Turing); (ii) unidirectional open-loop sensing yields at most transient focusing; (iii) bidirectional feedback reshapes the effective mobility M and yields stable, finite-band (Turing-type) niche formation, or aggregation/ill-posedness depending on strong parabolicity.

Keywords: Reaction-diffusion equation; tumor microenvironment; pharmacokinetics; open-loop therapy; chemotaxis; Turing instability; strong parabolicity; resistance niches.

1 Introduction

1.1 Background and motivation

Self-organized spatial heterogeneity is observed across physical, chemical, and biological systems, where it often emerges from the interplay between local reaction kinetics, spatial transport, and environmental signaling (Cross and Hohenberg 1993; Dolnik et al. 2001; Murray 2003; Colizza et al. 2007; Belik et al. 2011). A central goal in the nonlinear analysis of partial differential equations is to identify which structural mechanisms can generate spatial patterns from homogeneous equilibria, and which mechanisms instead enforce relaxation toward homogeneity. In this paper we focus on a mechanism-level question motivated by tumor microenvironment dynamics: under

strong damping (crowding/competition and signal relaxation), which coupling topologies can nevertheless amplify spatial perturbations into persistent heterogeneity, and which are intrinsically incapable of doing so?

The classical patterning paradigm is formulated as reaction–diffusion equations (Cherniha and Davydovych 2017; Kondo and Miura 2010),

$$\begin{cases} \partial_t X = d_1 \Delta X + a(X - h) + b(Y - k), \\ \partial_t Y = d_2 \Delta Y + c(X - h) + d(Y - k), \end{cases}$$

and, as initiated by Turing (Turing 1952), shows that diffusion may destabilize a stable homogeneous steady state and induce a diffusion-driven bifurcation to patterned states. This mechanism has been extensively studied, and rigorous theories of existence, stability, and bifurcation for nonlinear diffusion systems are now classical (Chen and Buceta 2019; Henry 1981; Smoller 1994).

Although classical Turing mechanisms generate spatial structures through diffusion-driven instabilities without requiring directed cell movement, pattern initiation in many biological systems is an active process in which cells sense, respond to, and amplify nascent spatial cues; the resulting directed migration then contributes directly to subsequent morphogenesis. Cell movement is therefore central to examples such as aggregation of the social amoeba *Dictyostelium discoideum* (Höfer et al. 1995), stripe formation in fish pigmentation (Painter et al. 1999), gastrulation and limb morphogenesis in the chick embryo (Li and Muneoka 1999; Yang et al. 2002), various bacterial aggregation phenomena (Budrene and Berg 1991, 1995), and primitive streak formation (Painter et al. 2000). In these cases the movements are typically elicited and guided by chemotactic responses to spatially varying signals, a process termed chemotaxis. The modeling of chemotaxis begins with the Keller–Segel formulation (Keller and Segel 1970, 1971; Murray 2002), which incorporates directed motion along chemical gradients:

$$\begin{cases} \partial_t n = f(n) - \nabla \cdot (n \chi(a) \nabla a) + \nabla \cdot D \nabla n, \\ \partial_t a = g(a, n) + \nabla \cdot D_a \nabla a. \end{cases} \quad (1)$$

While diffusion tends to smooth perturbations, chemotaxis can destabilize homogeneous states in suitable regimes, leading to aggregation, spatial patterning, or blow-up phenomena (Horstmann and Winkler 2005; Jin et al. 2026; Horstmann 2003; Arumugam and Tyagi 2021; Jäger and Luckhaus 1992). Subsequent refinements enhance mechanistic realism (Martiel and Goldbeter 1987; Goldbeter 2004; Monk and Othmer 1989; Spiro et al. 1997).

Nonlinear diffusion extensions further incorporate density-dependent interactions, including $D(u) = \mu_1 + \mu_2 u_m^4 / (u_m^2 + u^4)$ (critical density u_m) (Höfer et al. 1995), $D(u) = u^n$ ($n > 1$) (Kowalczyk 2005), $D(u) = 1 / (1 - u)^\alpha$ ($\alpha > 0$) (Choi and Wang 2010), and $D(u) = (1 + u) / (1 - u + u \ln u)$ (Lushnikov et al. 2008). Wang (Wang 2010)

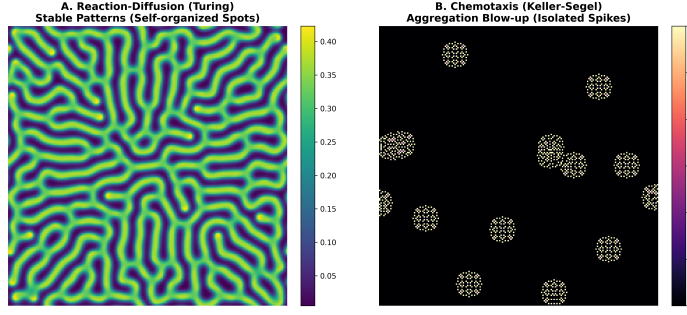


Fig. 2 Comparison of spatial instability mechanisms. (A) Diffusion-driven instability (Turing mechanism): interaction between local reaction kinetics and differential diffusion generates stable, self-organized spatial patterns (e.g., stripes) from a homogeneous state. (B) Aggregation-driven instability (chemotaxis mechanism): directed transport leads to mass concentration and blow-up phenomena (spots) rather than smooth spatial structures. This paper investigates the transition between these regimes.

synthesized these advances by introducing:

$$\begin{cases} \partial_t u = \nabla \cdot (D(u) \nabla u - \chi u \phi(u) \nabla v), \\ \partial_t v = D_v \Delta v + \mu u - \delta v. \end{cases}$$

The representative pairs

$$\begin{aligned} (D_1(u), \phi_1(u)) &= (d, 1), \\ (D_2(u), \phi_2(u)) &= (d, 1 - u), \\ (D_3(u), \phi_3(u)) &= (d(1 + (\gamma - 1)u^\gamma), 1 - u^\gamma), \quad (\gamma > 1), \\ (D_4(u), \phi_4(u)) &= (d(1 - u)^{r-1}(1 - u(1 - r)), (1 - u)^r), \quad (r > 1), \end{aligned}$$

demonstrate that directed transport can interact with diffusion and kinetics to produce finite-wavelength instabilities, while in other regimes it can drive concentration aggregation and blow-up rather than smooth tissue-scale patterns (Bubba et al. 2019; Wang 2010). Figure 2 illustrates this distinction: the left panel depicts diffusion-driven (Turing-type) patterning, whereas the right panel depicts an aggregation-driven instability with spike formation.

In tumor microenvironment settings, spatial organization is shaped not only by diffusion and taxis, but also by heterogeneous signaling, competitive interactions, and state transitions of both tumor and stromal compartments (Najafi et al. 2019; David et al. 2025; Zhang et al. 2024; Yuan 2016; Wells et al. 2015). Chemotaxis-based and reaction-diffusion models have been used to study tumor growth and invasion (Bubba et al. 2019; Watts et al. 2016; Puliafito et al. 2015), yet many formulations treat microenvironmental components in a reduced or decoupled manner that obscures the mechanism by which spatial heterogeneity is created or eliminated (Oudin and Weaver 2016; Esfahani et al. 2022). In particular, from a rigorous pattern-formation

perspective, the joint role of (i) competing tumor phenotypes, (ii) microenvironmental state transitions, and (iii) fast-relaxing exogenous inhibitory forcing has not been fully characterized. Hybrid multiscale oncology models provide a complementary route to connect tissue-scale transport fields with cell-level phenotypic dynamics and resistance evolution (Wang et al. 2025). These developments support the broader modeling strategy pursued here: identifying mechanism-level organizing principles in a tractable hybrid continuum framework, while clarifying how additional stochastic or agent-based structure could be incorporated in a mathematically controlled manner.

1.2 Model and biological interpretation

The above research gap motivates the present work. We develop a mathematically tractable hybrid PDE–ODE framework that couples competition between two tumor phenotypes to stromal state transitions, and includes an open-loop, single-dose therapeutic agent I that diffuses in space and is cleared in time. Figure 1 illustrates the coupling topology considered here. Our goal is mechanism-driven: under strong damping (crowding/competition and signal relaxation), when can directed transport generate spatial heterogeneity from a homogeneous equilibrium, and when is it structurally incapable of inducing diffusion-driven (Turing-type) bifurcation?

A closely related issue is physical realism. When feedback is sufficiently strong to overwhelm diffusive smoothing, unregularized continuum descriptions may predict aggregation/collapse rather than smooth, finite-wavelength structures, indicating the need for biologically motivated regularization (e.g. volume filling (Wrzosek 2010) or flux saturation (Chertock et al. 2012)). These themes guide both the modeling hierarchy and the analytical results developed in the remainder of the paper.

To study these questions in a form that supports rigorous analysis and transparent interpretation, we consider a hybrid reaction–diffusion PDE–ODE model on a bounded domain $U \subseteq \mathbb{R}^N$ ($N \in \{1, 2, 3\}$) with C^∞ boundary. Throughout the paper, we impose homogeneous Neumann boundary conditions (zero flux) for the diffusing species,

$$\partial_n S = \partial_n R = \partial_n I = 0 \quad \text{on } \partial U,$$

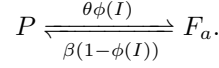
which represent a closed tissue region with no net exchange across the boundary. We assume nonnegative initial data, consistent with the interpretation of the state variables as densities and concentrations.

Base hybrid PDE–ODE system (no chemotaxis). We propose the following coupled system:

$$\begin{cases} \partial_t S = d_S \Delta S + \lambda_S S \left(1 - \frac{S+R}{K}\right) - \alpha S - \delta(I)S + \xi[1 - \phi(I)]R, & x \in U, t > 0, \\ \partial_t R = d_R \Delta R + \lambda_R R \left(1 - \frac{S+R}{K}\right) + \alpha S + \eta \phi(I)F_a R - \xi[1 - \phi(I)]R, & x \in U, t > 0, \\ \partial_t I = d_I \Delta I - \gamma_I I, & x \in U, t > 0, \\ \partial_t P = -\theta \phi(I)P + \beta[1 - \phi(I)]F_a, & x \in U, t > 0, \\ \partial_t F_a = \theta \phi(I)P - \beta[1 - \phi(I)]F_a, & x \in U, t > 0. \end{cases} \quad (2)$$

The densities $S(x, t)$ and $R(x, t)$ represent two competing tumor phenotypes, interpreted as therapy-susceptible and therapy-resistant populations, respectively. Both S and R undergo logistic growth with intrinsic rates λ_S, λ_R and a shared carrying capacity K , introducing strong damping through crowding and competition via the factor $1 - (S + R)/K$. The two phenotypes interconvert at rates α ($S \rightarrow R$) and ξ ($R \rightarrow S$), representing reversible switching under environmental pressure.

Stromal switching variables. To ground the microenvironmental variables in a concrete setting, we interpret (P, F_a) as two phenotypic states of the stromal fibroblast pool. Here $P(x, t)$ denotes the density of quiescent (inactive) fibroblasts, while $F_a(x, t)$ denotes the density of activated fibroblasts (e.g. cancer-associated fibroblasts (Sahai et al. 2020)). Activated fibroblasts modulate the local microenvironment via remodeling cues and growth-factor secretion. With this identification, the model couples three mechanisms central to tumor microenvironments: competition, signal-mediated regulation, and microenvironmental state transitions (Najafi et al. 2019; David et al. 2025; Zhang et al. 2024; Yuan 2016; Wells et al. 2015). The (P, F_a) subsystem has the structure of a two-state phenotypic conversion model with drug-dependent rates,



In the hybrid regime, we treat the stromal conversion variables (P, F_a) as effectively nonmotile on the pattern-formation time window and set

$$\partial_t P = -\theta \phi(I)P + \beta[1 - \phi(I)]F_a, \quad \partial_t F_a = \theta \phi(I)P - \beta[1 - \phi(I)]F_a, \quad x \in U, t > 0,$$

so that the P - and F_a -equations become pointwise ODEs coupled to the PDE components (S, R, I) . The conversion structures imply the pointwise conservation law $\partial_t(P + F_a) = 0$ (see Proposition 3.2). We interpret this as a short-timescale approximation: switching between quiescent and activated states occurs on a timescale faster than fibroblast proliferation or apoptosis, so that on the migration and pattern-formation window the total stromal density acts as a conserved local pool.

For longer timescales, stromal recruitment and turnover can be incorporated via small source–sink terms, e.g.

$$\partial_t P = \dots + s_P - \mu_P P, \quad \partial_t F_a = \dots + s_{F_a} - \mu_{F_a} F_a, \quad (3)$$

with $s_{P,F_a} \geq 0$ and $\mu_{P,F_a} \geq 0$. Our analysis focuses on the conservative switching limit, which provides the cleanest mechanism-level setting. Including moderate source–sink terms primarily shifts homogeneous equilibrium levels and is not expected to change the qualitative directionality–damping classification, provided the system remains in a well-posed parabolic regime.

Drug pharmacokinetics and signaling. The field $I(x, t)$ denotes the concentration of an exogenously administered therapeutic agent (single-dose chemotherapy drug). It diffuses through tissue and is cleared at rate γ_I , so that after dosing the drug relaxes exponentially. Repeated dosing or sustained delivery can be incorporated by adding an input term, which we do not pursue here. The drug I enters the tumor layer through an inhibitory term acting on S , modeled by Michaelis–Menten kinetics ([Cornish-Bowden 2015](#)),

$$\delta(I) = \delta_0 \frac{I}{I + K_I},$$

with maximal inhibition rate δ_0 and half-saturation concentration K_I . The same drug field controls stromal activation through a switch ϕ . We assume $\phi : \mathbb{R}_+ \rightarrow (0, 1)$ is smooth, bounded, and globally Lipschitz continuous. Additionally, we require $\phi(I) \approx 0$ for small I and $\phi(I) \approx 1$ for large I . A representative choice is

$$\phi(I) = \tanh(\kappa_\phi I), \quad \kappa_\phi > 0,$$

where κ_ϕ controls the steepness of the drug-dependent switch. Activated fibroblasts promote the resistant phenotype through the coupling term $\eta \phi(I) F_a R$, encoding the idea that drug-driven stromal activation can transiently create a niche that favors resistance ([Milne et al. 2025; Meads et al. 2009](#)). Figure 3 summarizes the resulting interaction topology.

Two modeling levels: baseline vs. chemotaxis extensions. We analyze two levels of description:

- (i) the base hybrid PDE–ODE system (2) (no chemotaxis), for which P, F_a is governed by pointwise ODEs, and yielding a conservative stromal pool; and
- (ii) chemotaxis-augmented extensions (Section 4), in which spatial gradients of a signal appear explicitly in the flux and therefore require sufficient spatial regularity of that signal. We denote the chemotactic signal by c and evolve it by a parabolic equation in the chemotaxis setting (e.g. $\partial_t c = d_c \Delta c + \mathcal{Q}(c)$).

Homogeneous pool branch. Governed by pointwise ODEs, the conserved quantity $P(x, t) + F_a(x, t) = P_0(x) + F_{a,0}(x)$ may be spatially heterogeneous, and the system admits a continuum of local steady states parameterized by this pool. In the stability

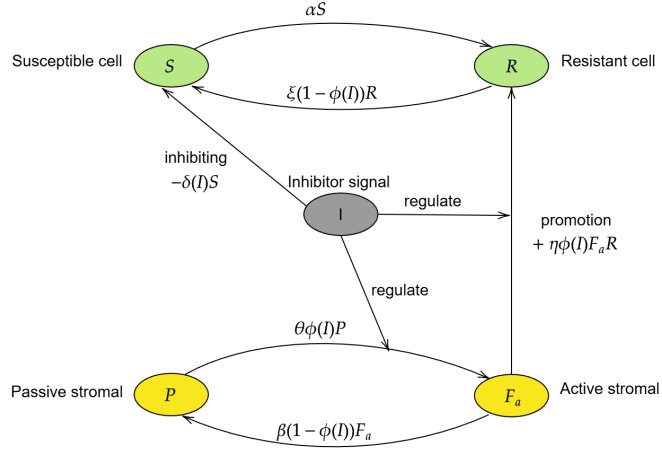


Fig. 3 Topology of the hybrid PDE–ODE interaction network. The inhibitor I acts as a central signaling hub connecting the tumor layer (S, R) and the microenvironmental layer (P, F_a). Key features include I providing negative feedback to S ($-\delta(I)S$) while activating the microenvironmental stromal cells via the switch $\phi(I)$. The switch promotes resistance via the $\eta\phi(I)F_aR$ term, creating a drug-gated feedback channel from stroma to the resistant phenotype.

and pattern-formation analysis below, we therefore restrict attention to the homogeneous branch corresponding to spatially constant total stromal density (see also the definition of homogeneous equilibrium in Section 3.5).

1.3 Main message and contributions: Bridging theory and clinical reality

This work is motivated by a recurring translational tension: clinically realistic interventions act as transient, open-loop forcings, whereas spatial resistance niches are often sustained by endogenous, feedback-mediated microenvironmental remodeling. Our central message is mechanism-level: in damped hybrid PDE–ODE systems, whether therapeutic perturbations relax toward homogeneity or instead permit spatial self-organization is determined by the interplay between coupling directionality (open-loop vs. closed-loop) and damping/relaxation structure (crowding competition, signal decay, and washout).

Unlike standard models that assume steady or sustained forcing, our framework incorporates the clinically relevant constraint of single-dose pharmacokinetics through a decaying inhibitor field I . In this stringent baseline, we show that directed transport can overcome relaxation only when it participates in a feedback loop that reshapes the effective transport operator—a structural insight that suggests testable hypotheses about when stromal crosstalk may support, or fail to support, persistent spatial heterogeneity.

Main results. For a bounded domain $U \subset \mathbb{R}^N$ with smooth boundary and homogeneous Neumann conditions, our analysis yields three contributions:

(R1) **Rigorous mathematical backbone for biological consistency.** For the base hybrid system (2), we establish global well-posedness and forward invariance of the biologically meaningful state space. Using quasi-positivity, we prove preservation of nonnegativity for all components. Global-in-time classical solutions are obtained via an L^∞ continuation (blow-up alternative) closed by explicit a priori bounds and comparison estimates. This ensures that any instability observed in later chemotaxis extensions reflects genuine dynamical behavior rather than finite-time mathematical pathology.

(R2) **Therapeutic washout limit and the baseline no-Turing conclusion.** We analyze the long-time reduction under realistic drug clearance,

$$\partial_t I = d_I \Delta I - \gamma_I I,$$

which implies exponential washout of the open-loop inhibitor. As $I(\cdot, t) \rightarrow 0$, all drug-mediated couplings vanish asymptotically and the dynamics reduce to the $I \equiv 0$ limit. In particular, the post-washout reaction–diffusion linearization of the tumor subsystem (S, R) about its homogeneous coexistence equilibrium admits no diffusion-driven Turing instability. Thus, in the damped baseline architecture, diffusion cannot destabilize homogeneity after the transient drug perturbation has relaxed. This establishes a stringent reference point for identifying which additional transport couplings can genuinely generate spatial structure.

(R3) **Directionality–damping principle for directed transport.** To model spatial reorganization, we introduce chemotaxis extensions and establish a dichotomy governed by coupling topology:

- (i) Unidirectional (open-loop) sensing. Populations respond to a relaxing signal field but do not regulate it. Under logistic damping and signal relaxation, such one-way coupling can produce at most transient focusing and cannot generate diffusion-driven patterns from a homogeneous equilibrium.
- (ii) Bidirectional (closed-loop) feedback. The signal depends on the populations, closing a feedback loop and modifying the effective mobility matrix. This yields explicit thresholds separating (a) a stable, well-posed regime, (b) a well-posed finite-band (Turing-type) instability regime associated with resistance-niche formation, and (c) an aggregation/ill-posed regime corresponding to loss of strong parabolicity and necessitating physical regularization.

This classification provides a mathematically explicit mechanism map linking feedback strength to the qualitative form of spatial instability.

Numerical validation. Reproducible simulations corroborate the analytical regimes: they confirm relaxation toward homogeneity in the base and unidirectional settings, demonstrate sustained finite-wavelength structure only under closed-loop feedback in the well-posed regime, and identify the regularization (e.g. flux limitation) required to obtain physically meaningful dynamics in the ill-posed regime.

Organization of the paper. Section 2 introduces the base hybrid system, the analytical setting, and the chemotaxis model classes. Section 3 establishes invariance, global well-posedness, the washout reduction, and the baseline no-Turing conclusion

for the post-washout (S, R) reaction–diffusion linearization. Section 4 develops the directionality–damping principle: unidirectional stability and the bidirectional classification into stable, finite-band (Turing-type), and aggregation/ill-posed regimes. Section 5 provides reproducible numerical evidence supporting the classification and illustrates a minimal feedback experiment that restores finite-wavelength patterning. We conclude in the Discussion with interpretation, limitations, and modeling extensions.

2 Model and Analytical Setting

2.1 Base hybrid PDE–ODE model (no chemotaxis)

We begin with the base hybrid PDE–ODE system (2) without chemotactic transport. This level of description isolates the competition–inhibition–conversion architecture and provides the analytical baseline for the mechanism results developed later. In particular, it allows us to establish invariance of the nonnegative cone, global well-posedness, long-time reduction under drug washout, and a baseline no-Turing conclusion for the damped reaction–diffusion core.

Let $U \subseteq \mathbb{R}^N$ ($N \in \{1, 2, 3\}$) be a bounded domain with C^∞ boundary ∂U . Throughout the paper, we impose homogeneous Neumann boundary conditions for the diffusing components (S, R, I) ,

$$\partial_n S = \partial_n R = \partial_n I = 0 \quad \text{on } \partial U \times (0, \infty), \quad (4)$$

corresponding to a closed tissue region with zero flux across the boundary.

Hybrid structure and baseline regime. The model (2) consists of reaction–diffusion equations for (S, R, I) coupled to a stromal conversion subsystem (P, F_a) , together with (4) and nonnegative initial data. In the hybrid regime, (P, F_a) evolves pointwise in space as an ODE subsystem driven by the drug-dependent switch $\phi(I)$. This conservative switching limit retains microenvironmental state transitions; small source–sink corrections can be incorporated on longer timescales as in (3).

Let $\mathbf{u} = (S, R, I, P, F_a)^\top$ and write (2) in the semilinear form

$$\partial_t \mathbf{u} - \mathcal{D}_{\text{diff}} \Delta \mathbf{u} = \mathcal{G}(\mathbf{u}), \quad \mathcal{D}_{\text{diff}} = \text{diag}(d_S, d_R, d_I, 0, 0), \quad (5)$$

where $\mathcal{G} = (G_1, \dots, G_5)^\top$ is given by

$$\begin{cases} G_1(\mathbf{u}) = \lambda_S S \left(1 - \frac{S+R}{K}\right) - \alpha S - \delta(I)S + \xi(1 - \phi(I))R, \\ G_2(\mathbf{u}) = \lambda_R R \left(1 - \frac{S+R}{K}\right) + \alpha S + \eta \phi(I)F_a R - \xi(1 - \phi(I))R, \\ G_3(\mathbf{u}) = -\gamma_I I, \\ G_4(\mathbf{u}) = -\theta \phi(I)P + \beta(1 - \phi(I))F_a, \\ G_5(\mathbf{u}) = \theta \phi(I)P - \beta(1 - \phi(I))F_a. \end{cases}$$

Here $\delta(I) = \delta_0 I / (I + K_I)$ is of Michaelis–Menten type (Cornish-Bowden 2015) and $\phi(I)$ is a smooth switch (see Section 1.2). On bounded subsets of $\mathbb{R}_{\geq 0}$ these nonlinearities are smooth, so the reaction map \mathcal{G} is locally Lipschitz. Table 1 summarizes key parameters.

Table 1 Key parameters, meanings, and units (final notation). Parameters marked by \dagger appear only in chemotaxis / feedback extensions.

Parameter	Meaning	Unit
Diffusion / transport		
d_S, d_R, d_I	diffusion coefficients of S, R, I	mm^2/s
d_c^\dagger	diffusion coefficient of chemoattractant c	mm^2/s
$\chi_S^\dagger, \chi_R^\dagger$	chemotactic sensitivity of S, R to ∇c (unidirectional/abstract templates)	$\text{mm}^2/(\text{s}\cdot\text{M})$
$\chi_S^{'\dagger}$	additional sensitivity of S to ∇c in the explicit feedback model	$\text{mm}^2/(\text{s}\cdot\text{M})$
α_c^\dagger	flux-saturation strength in $\nabla c / (1 + \alpha_c \nabla c)$	mm/M
Tumor kinetics (logistic competition and switching)		
λ_S, λ_R	intrinsic growth rates of S, R	$1/\text{s}$
K	shared carrying capacity for $S + R$	M
α	phenotype switching rate $S \rightarrow R$	$1/\text{s}$
ξ	phenotype switching rate $R \rightarrow S$ (drug-off switch)	$1/\text{s}$
η	promotion rate of R by activated stroma (coupling via A)	$1/(\text{s}\cdot\text{M})$
Drug dynamics and drug-mediated effects		
γ_I	drug clearance/decay rate in $\partial_t I = d_I \Delta I - \gamma_I I$	$1/\text{s}$
δ_0	maximal inhibition rate of S by drug (via $\delta(I)$)	$1/\text{s}$
K_I	half-saturation concentration in $\delta(I) = \delta_0 I / (I + K_I)$	M
κ_ϕ	steepness parameter in $\phi(I) = \tanh(\kappa_\phi I)$ (or analogous switch)	$1/\text{M}$
Stromal switching module (baseline hybrid regime)		
θ	activation rate $P \rightarrow A$ modulated by $\phi(I)$	$1/\text{s}$
β	deactivation rate $A \rightarrow P$ modulated by $1 - \phi(I)$	$1/\text{s}$
Chemoattractant dynamics (feedback experiments)		
κ_c^\dagger	production rate of chemoattractant c (e.g. $\kappa_c S$)	$1/\text{s}$
ρ_c^\dagger	decay rate of chemoattractant c	$1/\text{s}$

Assumption 2.1 (Homogeneous stromal pool). In the hybrid regime, the conversion (P, F_a) subsystem implies the pointwise conservation law $\partial_t(P + F_a) = 0$ and hence

$$P(x, t) + F_a(x, t) = P_0(x) + F_{a,0}(x) \quad \text{for all } t \geq 0.$$

When studying spatially homogeneous equilibria and their stability, we therefore restrict attention to initial data with spatially constant total stromal pool:

$$P_0(x) + F_{a,0}(x) \equiv P_T \quad \text{for some constant } P_T \geq 0. \quad (6)$$

This assumption ensures the existence of a homogeneous equilibrium branch in the baseline hybrid regime and will be imposed whenever homogeneous stability and pattern-formation criteria are invoked.

2.2 Weak formulation and function spaces

Fix $T > 0$ and denote $U_T := U \times (0, T]$. Following standard parabolic theory (Evans 2022; Amann 1995), we formulate weak solutions for the diffusing variables (S, R, I) under homogeneous Neumann boundary conditions. Let

$$V_{\mathfrak{N}}(T) := L^2(0, T; H^1(U)) \cap H^1(0, T; (H^1(U))'),$$

and seek

$$S, R, I \in V_{\mathfrak{N}}(T).$$

In the hybrid regime, the stromal conversion variables (P, F_a) evolve pointwise in space as an ODE subsystem driven by $\phi(I)$. Accordingly, we assume

$$P, F_a \in C^1([0, T]; L^2(U)),$$

which is compatible with the ODE structure and with the pointwise conservation law for $P + F_a$ (see Proposition 3.2).

Weak formulation. Let $\mathbf{u} = (S, R, I, P, F_a)^\top$ and let $\mathcal{G}(\mathbf{u}) = (G_1, \dots, G_5)^\top$ be the reaction field in (5). A quintuple (S, R, I, P, F_a) is a weak solution on $(0, T)$ if S, R, I and P, F_a satisfy the above regularity and, for every test function

$$\varphi = (\varphi_S, \varphi_R, \varphi_I) \in [V_{\mathfrak{N}}(T)]^3$$

and for a.e. $t \in (0, T)$, the following identities hold:

$$\begin{aligned} \langle \partial_t S, \varphi_S \rangle + d_S(\nabla S, \nabla \varphi_S)_{L^2(U)} &= (G_1(\mathbf{u}), \varphi_S)_{L^2(U)}, \\ \langle \partial_t R, \varphi_R \rangle + d_R(\nabla R, \nabla \varphi_R)_{L^2(U)} &= (G_2(\mathbf{u}), \varphi_R)_{L^2(U)}, \\ \langle \partial_t I, \varphi_I \rangle + d_I(\nabla I, \nabla \varphi_I)_{L^2(U)} &= (G_3(\mathbf{u}), \varphi_I)_{L^2(U)}. \end{aligned} \quad (7)$$

Here $(\cdot, \cdot)_{L^2(U)}$ denotes the $L^2(U)$ inner product and $\langle \cdot, \cdot \rangle$ denotes the duality pairing between $H^1(U)$ and $(H^1(U))'$. The homogeneous Neumann boundary conditions $\partial_n S = \partial_n R = \partial_n I = 0$ are encoded in the integration-by-parts step leading to (7).

Initial data. We assume nonnegative initial data

$$\mathbf{u}_0 = (S_0, R_0, I_0, P_0, F_{a,0}) \in (L^\infty(U))^5, \quad \mathbf{u}_0 \geq 0 \text{ a.e. in } U.$$

2.3 Chemotaxis extensions and well-definedness assumptions

Starting from the base system (2), we introduce Keller–Segel-type fluxes for S and R along gradients of a signal field c . We use c exclusively for chemotactic signaling.

Since the fluxes depend on ∇c , well-definedness requires sufficient spatial regularity of c , which we obtain by evolving c via a parabolic relaxation equation.

Unidirectional (open-loop) sensing. We first consider a one-way coupling in which tumor populations respond to the signal c but do not regulate it. In this open-loop setting, the signal dynamics are independent of (S, R) and relax in time. A concrete tumor–drug–stroma unidirectional extension takes the form

$$\begin{cases} \partial_t S = d_S \Delta S - \chi_S \nabla \cdot (S \nabla c) + \lambda_S S \left(1 - \frac{S+R}{K}\right) - \alpha S - \delta(I)S + \xi(1 - \phi(I))R, \\ \partial_t R = d_R \Delta R - \chi_R \nabla \cdot (R \nabla c) + \lambda_R R \left(1 - \frac{S+R}{K}\right) + \alpha S + \eta \phi(I)F_a R - \xi(1 - \phi(I))R, \\ \partial_t c = w d_c \Delta c + \mathcal{Q}(c), \quad \partial_c \mathcal{Q}(c) < 0, \end{cases} \quad (8)$$

with the remaining components (I, P, F_a) evolving as in (2). The condition $\partial_c \mathcal{Q} < 0$ encodes signal decay/relaxation and provides a damping mechanism that competes against chemotactic focusing.

In the single-dose setting, Proposition 3.2 implies $I(\cdot, t) \rightarrow 0$ exponentially, hence $\delta(I)$ and $\phi(I)$ vanish asymptotically. Therefore, the mode-wise stability question near the long-time homogeneous state reduces to an autonomous (S, R) kinetics, and we isolate the transport mechanism via the templates (9)–(10). Appendix A details rigorous mathematical derivations for such reduction and justify the drug-free dynamics in (9)–(10) as a chemotaxis extension of (2). To emphasize transferability beyond the specific tumor–drug–stroma nonlinearities, we also consider the damped unidirectional templates

$$\begin{cases} \partial_t S = d_S \Delta S - \chi_S \nabla \cdot (S \nabla c) + \lambda_S S \left(1 - \frac{S+R}{K}\right) + f_S(S, R), \\ \partial_t R = d_R \Delta R - \chi_R \nabla \cdot (R \nabla c) + \lambda_R R \left(1 - \frac{S+R}{K}\right) + f_R(S, R), \\ \partial_t c = d_c \Delta c + \mathcal{Q}(c), \quad \partial_c \mathcal{Q}(c) < 0, \end{cases} \quad (9)$$

and its abstract counterpart

$$\begin{cases} \partial_t S = d_S \Delta S - \chi_S \nabla \cdot (S \nabla c) + f_S(S, R), \\ \partial_t R = d_R \Delta R - \chi_R \nabla \cdot (R \nabla c) + f_R(S, R), \\ \partial_t c = d_c \Delta c + \mathcal{Q}(c), \quad \partial_c \mathcal{Q}(c) < 0. \end{cases} \quad (10)$$

Bidirectional (closed-loop) feedback. To model settings in which the populations actively shape the guiding signal, we consider feedback systems in which the signal landscape depends on (S, R) . A convenient abstraction—sufficient for the linearized mechanism classification developed later—is the closed-loop class

$$\begin{cases} \partial_t S = d_S \Delta S - \chi_S \nabla \cdot (S \nabla g(S, R)) + f_S(S, R), \\ \partial_t R = d_R \Delta R - \chi_R \nabla \cdot (R \nabla g(S, R)) + f_R(S, R), \end{cases} \quad (11)$$

where $g(S, R)$ represents a feedback-generated signal landscape. In this class, spatial inhomogeneities in (S, R) generate gradients in $g(S, R)$ that further bias transport, providing a closed-loop amplification mechanism that is absent in the unidirectional case.

Well-definedness assumptions. In the unidirectional setting (8)–(10), the parabolic evolution of c ensures ∇c is well-defined (in the weak sense) whenever $c \in L^2(0, T; H^1(U))$. In the bidirectional abstraction (11), the fluxes are written directly in terms of $\nabla g(S, R)$. Accordingly, we assume $g \in C^1(\mathbb{R}^2)$ and work near sufficiently regular solutions so that the compositions $g(S, R)$ and $\nabla g(S, R)$ are meaningful; the stability analysis in Section 4 is carried out at smooth homogeneous equilibria, where these requirements are satisfied.

3 Base Model Analysis

3.1 Invariant region and nonnegativity

We first record the forward-invariant region underlying the base hybrid system (2). Many variants about standard positivity/invariance results for semilinear parabolic systems with homogeneous Neumann boundary conditions appear in the literature; see, e.g., (Amann 1995; Smoller 1994). Since the state variables represent densities and concentrations, the physically meaningful phase space is the nonnegative cone. The result below establishes preservation of nonnegativity for all components under the standing Neumann boundary condition (4).

Theorem 3.1 (Nonnegativity) *Let $U \subseteq \mathbb{R}^N$ ($N \in \{1, 2, 3\}$) be a bounded domain with C^∞ boundary, and consider the base system (2) under homogeneous Neumann boundary conditions*

$$\partial_n S = \partial_n R = \partial_n I = 0 \quad \text{on } \partial U \times (0, \infty).$$

Assume that all parameters in (2) are nonnegative constants and that the initial data satisfy

$$S_0, R_0, I_0, P_0, F_{a,0} \geq 0 \quad \text{a.e. in } U, \quad (S_0, R_0, I_0, P_0, F_{a,0}) \in (L^\infty(U))^5.$$

Then any classical solution $\mathbf{u} = (S, R, I, P, F_a)$ of (2) on its maximal interval of existence $[0, T_{\max})$ remains nonnegative:

$$S(x, t), R(x, t), I(x, t), P(x, t), F_a(x, t) \geq 0 \quad \text{for all } (x, t) \in \overline{U} \times [0, T_{\max}).$$

Proof Step 1: Quasi-positivity. Let $\mathcal{G} = (G_1, \dots, G_5)^\top$ be as in (5) with $\mathbf{u} = (S, R, I, P, F_a)^\top$. We verify that \mathcal{G} is quasi-positive on $\mathbb{R}_{\geq 0}^5$: for each component i , if $u_i = 0$ and $\mathbf{u} \geq 0$, then $G_i(\mathbf{u}) \geq 0$. Indeed, for $\mathbf{u} \geq 0$,

$$\begin{aligned} G_1|_{S=0} &= \xi(1 - \phi(I))R \geq 0, \\ G_2|_{R=0} &= \alpha S \geq 0, \\ G_3|_{I=0} &= 0, \\ G_4|_{P=0} &= \beta(1 - \phi(I))F_a \geq 0, \\ G_5|_{F_a=0} &= \theta\phi(I)P \geq 0, \end{aligned}$$

since $\phi(I) \in (0, 1)$ and all parameters are nonnegative.

Step 2: Positivity of the diffusing components (S, R, I) . Let $\mathbf{u} = (S, R, I)$. We define the maximal interval of nonnegativity as

$$\tau := \sup \{t \in [0, T_{\max}) : S(\cdot, s), R(\cdot, s), I(\cdot, s) \geq 0 \text{ on } \bar{U} \text{ for all } s \in [0, t]\}.$$

We claim that $\tau = T_{\max}$. Suppose, for the sake of contradiction, that $\tau < T_{\max}$. By the definition of τ and continuity, we have:

- (i) $S(x, t) \geq 0$, $R(x, t) \geq 0$, and $I(x, t) \geq 0$ for all $x \in \bar{U}$ and $t \in [0, \tau]$.
- (ii) There exists a component (without loss of generality, assume S) and a point $x^* \in \bar{U}$ such that $S(x^*, \tau) = 0$.

At the point (x^*, τ) , S attains a global spatial minimum (value 0). If $x^* \in U$, then $\Delta S(x^*, \tau) \geq 0$ by the standard necessary condition for a minimum. We next show that the same sign condition holds if $x^* \in \partial U$. The homogeneous Neumann boundary condition,

$$\partial_n S(x^*, \tau) = \nabla S(x^*, \tau) \cdot n(x^*) = 0,$$

implies that the gradient of S at x^* lies in the tangent space $T_{x^*} \partial U$, where $n(x^*)$ is the unit outward normal vector of ∂U at x^* . Taylor expansion about S at x^* gives

$$S(x, \tau) = S(x^*, \tau) + \nabla S(x^*, \tau) \cdot (x - x^*) + \frac{1}{2}(x - x^*)^\top H S(x^*, \tau)(x - x^*) + o(\|x - x^*\|^2),$$

where $H S(x^*, \tau)$ is the Hessian matrix of S at x^* . The minimum at x^* implies that either

$$\nabla S(x^*, \tau) \cdot (x - x^*) \geq 0, \quad (12)$$

or,

$$\nabla S(x^*, \tau) \cdot (x - x^*) = 0 \text{ and } \frac{1}{2}(x - x^*)^\top H S(x^*, \tau)(x - x^*) \geq 0 \quad (13)$$

Let $x \in U$, we define a projection operator:

$$T_0 : U \rightarrow T_{x^*} \partial U$$

$$x \mapsto (x - x^*) + (n(x^*) \cdot (x - x^*)) n(x^*).$$

$T_0(x)$ is the projection of $x - x^*$ onto the tangent space $T_{x^*} \partial U$. Since U is a bounded domain with C^∞ boundary ∂U , it is easy to see the linear span of $T_0(x)$ for $x \in U$ is the whole tangent space:

$$\text{span}_{\mathbb{R}}\{T_0(x) : x \in U\} = T_{x^*} \partial U.$$

(12) and $\nabla S(x^*, \tau) \in T_{x^*} \partial U$ ensure that $\nabla S(x^*, \tau) = 0$. (13) ensures that $H S(x^*, \tau)$ is positive semidefinite. Therefore, we have for $x^* \in \partial U$,

$$\Delta S(x^*, \tau) \geq 0.$$

Going back to the S -equation at (x^*, τ) :

$$\partial_t S(x^*, \tau) = d_S \Delta S(x^*, \tau) + G_1(S = 0) \geq 0.$$

Therefore, S cannot become negative in the immediate future $t > \tau$. This contradiction implies $\tau = T_{\max}$.

Step 3: Positivity of the stromal ODE subsystem (P, F_a) . For each fixed $x \in U$ the stromal variables satisfy the linear ODE system

$$\frac{d}{dt} \begin{pmatrix} P(x, t) \\ A(x, t) \end{pmatrix} = B(I(x, t)) \begin{pmatrix} P(x, t) \\ A(x, t) \end{pmatrix}, \quad B(I) = \begin{pmatrix} -\theta\phi(I) & \beta(1 - \phi(I)) \\ \theta\phi(I) & -\beta(1 - \phi(I)) \end{pmatrix}. \quad (14)$$

Note that $B(I)$ is a Metzler matrix for every $I \geq 0$ (its off-diagonal entries are nonnegative).

Fix $x \in U$ and write $p(t) = P(x, t)$, $a(t) = A(x, t)$. If $p(t_0) = 0$ at some time t_0 with $a(t_0) \geq 0$, then from (14),

$$p'(t_0) = \beta(1 - \phi(I(x, t_0))) a(t_0) \geq 0,$$

so p cannot decrease below 0 at t_0 . Similarly, if $a(t_0) = 0$ with $p(t_0) \geq 0$, then

$$a'(t_0) = \theta\phi(I(x, t_0)) p(t_0) \geq 0,$$

so a cannot decrease below 0 at t_0 . Hence the nonnegative quadrant in (p, a) is forward invariant, proving the claim.

Combining Steps 2 and 3 yields nonnegativity of all components on $\bar{U} \times [0, T_{\max}]$. \square

3.2 A priori bounds for the drug and stromal subsystem

The base hybrid model (2) contains two structural features that provide robust a priori control on the maximal existence interval: (i) the drug field I satisfies a decoupled linear parabolic equation with clearance, and (ii) in the hybrid regime, the stromal conversion subsystem (P, F_a) is conservative and bounded. We record these bounds in a form used repeatedly in the global continuation and long-time asymptotics arguments.

Proposition 3.2 (Bounds for (I, P, F_a)) *Let $\mathbf{u} = (S, R, I, P, F_a)$ be a classical solution of (2) on its maximal interval of existence $[0, T_{\max}]$, under homogeneous Neumann boundary conditions for (S, R, I) and with nonnegative initial data $\mathbf{u}_0 \in (L^\infty(U))^5$.*

(i) **Drug decay and L^∞ control.** The drug satisfies

$$\|I(t)\|_{L^\infty(U)} \leq e^{-\gamma_I t} \|I_0\|_{L^\infty(U)} \quad \text{for all } t \in [0, T_{\max}]. \quad (15)$$

(ii) **Pointwise conservation of the stromal pool.** For all $(x, t) \in U \times [0, T_{\max}]$,

$$P(x, t) + F_a(x, t) = P_0(x) + F_{a,0}(x). \quad (16)$$

In particular,

$$0 \leq P(x, t), F_a(x, t) \leq P_0(x) + F_{a,0}(x) \quad \text{for all } (x, t) \in U \times [0, T_{\max}]. \quad (17)$$

(iii) **Uniform L^∞ boundedness of (I, P, F_a) .** For all $t \in [0, T_{\max}]$,

$$\|I(t)\|_{L^\infty(U)} + \|P(t)\|_{L^\infty(U)} + \|F_a(t)\|_{L^\infty(U)} \leq \|I_0\|_{L^\infty(U)} + \|P_0\|_{L^\infty(U)} + \|F_{a,0}\|_{L^\infty(U)}. \quad (18)$$

Proof (i) **Drug decay.** The drug equation is

$$\partial_t I = d_I \Delta I - \gamma_I I \quad \text{in } U \times (0, T_{\max}), \quad \partial_n I = 0 \quad \text{on } \partial U \times (0, T_{\max}).$$

Define $J(x, t) := e^{\gamma_I t} I(x, t)$. Then J solves $\partial_t J = d_I \Delta J$ with homogeneous Neumann boundary condition, hence by the maximum principle,

$$\|J(t)\|_{L^\infty(U)} \leq \|J(0)\|_{L^\infty(U)} = \|I_0\|_{L^\infty(U)}.$$

Multiplying back by $e^{-\gamma_I t}$ yields (15).

(ii) **Conservation of $P + F_a$.** In the hybrid regime, summing the P - and F_a -equations in (2) gives $\partial_t(P + F_a) = 0$ pointwise, which implies (16). Together with nonnegativity (Theorem 3.1), this yields (17).

(iii) **Uniform L^∞ bound.** The estimate (18) follows by combining (15) with (17) and taking $L^\infty(U)$ norms. \square

Remark 3.3. The bounds in Proposition 3.2 identify the key invariant structure used in the global continuation argument: I is uniformly controlled and decays exponentially, while the stromal pool $P + F_a$ is conserved pointwise and hence (P, F_a) remain uniformly bounded on $[0, T_{\max}]$.

3.3 Well-posedness and global-in-time solutions

We next establish global well-posedness for the base hybrid system (2) under homogeneous Neumann boundary conditions. The argument follows a standard semigroup framework for semilinear parabolic systems: local existence and uniqueness are standard; global continuation then follows once finite-time blow-up in the L^∞ norm is excluded. The invariant-region bounds from Sections 3.1–3.2, in particular the a priori control of (I, P, F_a) and comparison bounds for (S, R) , provide the key input for the continuation step. To state the global result, we use the standard blow-up alternative for mild solutions in $L^\infty(U)$; we omit semigroup technicalities and refer to standard sources (e.g. (Amann 1995; Evans 2022)) for the abstract framework.

Theorem 3.4 (Global existence of mild solutions and classical regularity) (Rothe 1984) *Let $U \subseteq \mathbb{R}^N$ ($N \in \{1, 2, 3\}$) be a bounded C^∞ domain. Consider the base system (2) under homogeneous Neumann boundary conditions for (S, R, I) and assume nonnegative initial data*

$$\mathbf{u}_0 = (S_0, R_0, I_0, P_0, F_{a,0}) \in (L^\infty(U))^5, \quad \mathbf{u}_0 \geq 0 \text{ a.e. in } U.$$

Then:

(i) **Global mild well-posedness.** There exists a unique global-in-time mild solution

$$\mathbf{u}(\cdot, t) = (S(\cdot, t), R(\cdot, t), I(\cdot, t), P(\cdot, t), F_a(\cdot, t)) \in (L^\infty(U))^5 \quad \text{for all } t \geq 0.$$

(ii) **Classical regularity under Hölder initial data.** If, in addition,

$$(S_0, R_0, I_0) \in (C^{2+\alpha}(\bar{U}))^3, \quad (P_0, F_{a,0}) \in (C^\alpha(\bar{U}))^2, \quad 0 < \alpha < 1, \quad (19)$$

and the Neumann compatibility conditions hold,

$$\partial_n S_0 = \partial_n R_0 = \partial_n I_0 = 0 \quad \text{on } \partial U,$$

then the mild solution is classical. More precisely,

$$S, R, I \in C^{2+\alpha, 1+\alpha/2}(\bar{U} \times [0, \infty)), \quad P, F_a \in C^{\alpha, 1+\alpha/2}(\bar{U} \times [0, \infty)),$$

where for P, F_a the time regularity is inherited from the pointwise ODE structure in the baseline hybrid regime.

See (Ladyženskaja et al. 1968) for the definition of these Hölder spaces.

Proof Rothe et al. establish the unique mild solution for the semilinear parabolic equations on the maximal interval of existence $[0, T_{\max}]$ with $T_{\max} \in (0, \infty]$ with classical properties stated in (ii), and the following alternative:

$$\lim_{t \rightarrow T_{\max}^-} \|\mathbf{u}(t)\|_{L^\infty(U)} = \infty \quad \text{if } T_{\max} < \infty. \quad (20)$$

We show that for every $T < T_{\max}$,

$$\sup_{0 \leq t \leq T} \|\mathbf{u}(t)\|_{L^\infty(U)} \leq C_T \quad \text{with} \quad \lim_{t \rightarrow T_{\max}^-} C_T < \infty,$$

closing the proof and ensuring $T_{\max} = \infty$.

(i) Uniform control of (I, P, F_a) . By Proposition 3.2, (I, P, F_a) are uniformly bounded on $[0, T_{\max}]$. In particular,

$$\|F_a(t)\|_{L^\infty(U)} \leq F_{a,\max} := \|P_0\|_{L^\infty(U)} + \|F_{a,0}\|_{L^\infty(U)} \quad \text{for all } t \in [0, T_{\max}). \quad (21)$$

(ii) Comparison bounds for (S, R) . By Theorem 3.1, $S, R, I, P, F_a \geq 0$ on $\overline{U} \times [0, T_{\max}]$. Using $0 \leq \phi(I) \leq 1$ and $\delta(I) \geq 0$, and dropping nonpositive terms in (2), we obtain the pointwise inequalities

$$\partial_t S - d_S \Delta S \leq \lambda_S S + \xi R, \quad (22)$$

$$\partial_t R - d_R \Delta R \leq \alpha S + (\lambda_R + \eta F_{a,\max}) R. \quad (23)$$

Let $(\bar{s}(t), \bar{r}(t))$ solve the linear ODE system

$$\frac{d}{dt} \begin{pmatrix} \bar{s} \\ \bar{r} \end{pmatrix} = \begin{pmatrix} \lambda_S & \xi \\ \alpha & \lambda_R + \eta F_{a,\max} \end{pmatrix} \begin{pmatrix} \bar{s} \\ \bar{r} \end{pmatrix}, \quad \begin{pmatrix} \bar{s}(0) \\ \bar{r}(0) \end{pmatrix} = \begin{pmatrix} \|S_0\|_{L^\infty(U)} \\ \|R_0\|_{L^\infty(U)} \end{pmatrix}. \quad (24)$$

Since (\bar{s}, \bar{r}) are spatially constant, they define a supersolution pair for (22)–(23). By the parabolic comparison principle under homogeneous Neumann boundary conditions, it follows that

$$S(\cdot, t) \leq \bar{s}(t), \quad R(\cdot, t) \leq \bar{r}(t) \quad \text{for all } t \in [0, T].$$

Because (24) is linear with constant coefficients, (\bar{s}, \bar{r}) exist globally and grow at most exponentially. Hence for each fixed $T < T_{\max}$ there is a constant $C_T < \infty$ such that

$$\sup_{0 \leq t \leq T} (\|S(t)\|_{L^\infty(U)} + \|R(t)\|_{L^\infty(U)}) \leq C_T.$$

Combining (i) and (ii) yields $\sup_{0 \leq t \leq T} \|\mathbf{u}(t)\|_{L^\infty(U)} < \infty$ for every $T < T_{\max}$. By the blow-up alternative for maximal mild solutions in $L^\infty(\overline{U})$, this excludes finite-time blow-up and therefore $T_{\max} = \infty$. \square

Remark 3.5 (Mechanism behind global continuation). The continuation argument hinges on two structural damping features in (2): (i) the drug field I is uniformly controlled and decays exponentially, and (ii) the stromal conversion subsystem (P, F_a) is conservative and uniformly bounded in the baseline hybrid regime. These properties provide a priori control that prevents finite-time blow-up of the remaining components and supports global-in-time well-posedness.

3.4 Long-time reduction and global attractivity of the homogeneous equilibrium

We now characterize the long-time behavior of the base hybrid model (2) under open-loop, single-dose drug forcing. The key structural feature is that the drug field I evolves independently as a linear parabolic equation with clearance and therefore decays exponentially. Since the I -dependent couplings enter the remaining dynamics only through $\delta(I)$ and $\phi(I)$, the washout of I implies that these couplings vanish asymptotically. As a consequence, the dominant long-time phenotypic composition is organized under the $I \equiv 0$ limit, in which we can close the tumor subsystem as an autonomous ODE for (S, R) under the homogeneous limit $d_S = d_R = 0$.

Drug relaxation and asymptotic decoupling. By Proposition 3.2(i), the drug satisfies

$$\|I(t)\|_{L^\infty(U)} \leq e^{-\gamma_I t} \|I_0\|_{L^\infty(U)} \quad \text{for all } t \geq 0,$$

and hence $I(\cdot, t) \rightarrow 0$ exponentially as $t \rightarrow \infty$. Moreover, since $\phi(I) \rightarrow 0$ as $I \rightarrow 0$ and $\delta(I) = \delta_0 I / (I + K_I)$ satisfies $\delta(I) \sim (\delta_0 / K_I)I$ as $I \rightarrow 0$, all I -mediated interaction terms in (2) decay exponentially in time. In the baseline hybrid system (2), the stromal subsystem is uniformly bounded and the stromal pool is conserved pointwise (Proposition 3.2(ii)).

Interpretation. Under homogeneous Neumann boundary conditions, diffusion preserves spatial averages and tends to damp spatial inhomogeneities. When $I(\cdot, t) \rightarrow 0$ uniformly, the reaction terms converge uniformly to their $I = 0$ limits, so the local kinetics at different locations become asymptotically aligned. This motivates studying the homogeneous $I \equiv 0$ reduction as the organizing long-time limit for phenotypic composition. (We do not claim a global PDE convergence result here; rather, the reduction identifies the limiting kinetics and provides the reference equilibrium used in the subsequent linear Turing stability analysis.)

Reduced homogeneous dynamics after washout. In the homogeneous limit (and in the absence of sustained drug input), the population dynamics reduce to

$$\begin{cases} \frac{dS}{dt} = f_S(S, R) := \lambda_S S \left(1 - \frac{S+R}{K}\right) - \alpha S + \xi R, \\ \frac{dR}{dt} = f_R(S, R) := \lambda_R R \left(1 - \frac{S+R}{K}\right) + \alpha S - \xi R. \end{cases} \quad (25)$$

Besides the trivial equilibrium $\mathbb{K}_0 = (0, 0)$, this system has an interior coexistence equilibrium

$$\mathbb{K}^* = (S^*, R^*) = \left(\frac{\xi K}{\alpha + \xi}, \frac{\alpha K}{\alpha + \xi} \right), \quad \alpha + \xi > 0,$$

which represents the long-term phenotypic composition selected after drug washout.

Theorem 3.6 (Global attractivity of the coexistence equilibrium) *Assume $\alpha + \xi > 0$. Then the equilibrium \mathbb{K}^* of (25) is globally asymptotically stable in the positive quadrant.*

Proof Consider the Lyapunov function

$$V(S, R) = (S + R - K)^2.$$

Along solutions of (25), a direct calculation gives

$$\dot{V}(S, R) = -2K^{-1}(S + R - K)^2(\lambda_S S + \lambda_R R) \leq 0. \quad (26)$$

Moreover,

$$\dot{V}(S, R) = 0 \iff S + R = K,$$

since $\lambda_S S + \lambda_R R \geq 0$ in the positive quadrant. For each $r > 0$, the sublevel set

$$\Omega_r = \{(S, R) : V(S, R) \leq r\}$$

is compact and positively invariant. Let

$$E_r = \{(S, R) \in \Omega_r : \dot{V}(S, R) = 0\} = \{(S, R) : S + R = K\}.$$

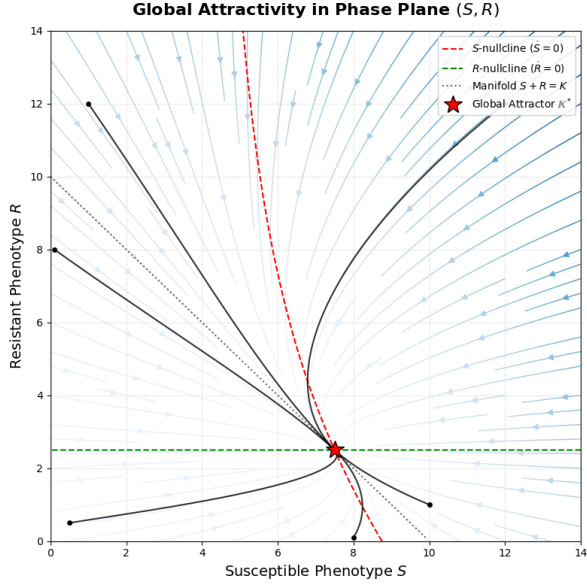


Fig. 4 Phase portrait of the reduced (S, R) subsystem. Red and green dashed lines depict the S - and R -nullclines, respectively. The black dashed line shows the one-dimensional invariant manifold $S + R = K$, where the S and R populations reach the carrying capacity K . The solid arrows demonstrate the direction and relative magnitude of the vector field, indicating the attractivity of the unique steady state \mathbb{K}^* that is represented by the red pentagram. Representative trajectories starting from the block dots approach \mathbb{K}^* . Parameters: $K = 10$, $\lambda_S = 0.8$, $\lambda_R = 0.4$, $\alpha = 0.1$, $\xi = 0.3$.

By LaSalle's invariance principle (LaSalle 1960; Haddad and Chellaboina 2011), every solution starting in Ω_r approaches the largest invariant subset of E_r as $t \rightarrow \infty$. On the invariant line $S + R = K$, the dynamics reduce to the scalar linear ODE

$$\frac{dS}{dt} = \xi(K - S) - \alpha S = \xi K - (\alpha + \xi)S,$$

which has the unique equilibrium $S^* = \xi K / (\alpha + \xi)$ and is globally attracting on $[0, K]$. Consequently, the largest invariant subset of E_r is $\{\mathbb{K}^*\}$, and thus $(S(t), R(t)) \rightarrow \mathbb{K}^*$ as $t \rightarrow \infty$. \square

Figure 4 illustrates the phase portrait of the reduced (S, R) subsystem (25). Vector fields point toward the unique steady state \mathbb{K}^* , showing the global stability of \mathbb{K}^* and validating the prediction of Theorem 3.6. The long-time reduction is consistent with a broader phenomenon in feedback-regulated compartmental models, where integrating the structured dynamics yields balanced laws for total populations and an autonomous ODE limit system whose equilibria organize stability behaviors (Liang et al. 2025).

Remark 3.7 (Phenotypic composition and a diagnostic ratio). The explicit expression for \mathbb{K}^* implies a simple diagnostic for the long-time phenotypic composition:

$$\rho := \frac{S^*}{R^*} = \frac{\xi}{\alpha}.$$

Thus $\rho \gg 1$ corresponds to an S -dominated regime, $\rho \ll 1$ to an R -dominated regime, and $\rho \approx 1$ to balanced coexistence. This ratio will be used later to interpret how additional couplings (including chemotaxis and feedback) can shift the system between regimes.

In summary, the open-loop drug field relaxes exponentially, so the I -mediated couplings in (2) vanish asymptotically. The reduced homogeneous dynamics (25) therefore captures the long-time phenotypic composition selected after drug washout. This equilibrium provides the reference point for the Neumann linear stability and mechanism classification developed in Section 4.

3.5 No diffusion-driven instability in the damped base model (Turing stability)

Definition 3.8 (Homogeneous equilibrium). In the following analysis, by a homogeneous equilibrium we mean a steady state

$$(S^*, R^*, I^*, P^*, F_a^*)$$

such that all components are spatially constant on U .

A key baseline conclusion for (2) is that its damping architecture does not support classical diffusion-driven (Turing-type) pattern generation after drug washout. Near the coexistence state selected by the $I \equiv 0$ limit, both tumor populations experience net negative feedback through logistic competition and switching, while diffusion under homogeneous Neumann boundary conditions acts as a smoothing mechanism. We formalize this by showing that no non-constant Neumann Laplacian mode can acquire positive growth rate for any choice of diffusion coefficients $d_S, d_R > 0$.

Theorem 3.9 (Turing stability of the reduced (S, R) subsystem) *Assume $\alpha + \xi > 0$ and let $\mathbb{K}^* = (S^*, R^*)$ be the interior coexistence equilibrium of the reduced homogeneous system (25). Consider the reaction-diffusion linearization of the (S, R) subsystem under homogeneous Neumann boundary conditions. Let $\mu = \lambda_k \geq 0$ denote a Neumann Laplacian eigenvalue on U (so that, on simple domains, $\mu = k^2$ with k the wavenumber). Then for every $\mu > 0$ all spectral growth rates satisfy $\Re \lambda(\mu) < 0$. In particular, there is no diffusion-driven (Turing-type) instability: homogeneity cannot be destabilized by diffusion.*

Proof Linearizing (25) at \mathbb{K}^* yields the Jacobian matrix \mathcal{J} with

$$\text{tr}(\mathcal{J}) = \partial_S f_S(\mathbb{K}^*) + \partial_R f_R(\mathbb{K}^*) = -\frac{\xi \lambda_S + \alpha \lambda_R}{\alpha + \xi} - \alpha - \xi < 0, \quad \det(\mathcal{J}) = \xi \lambda_S + \alpha \lambda_R > 0.$$

Moreover, the diagonal entries satisfy $\partial_S f_S(\mathbb{K}^*) < 0$ and $\partial_R f_R(\mathbb{K}^*) < 0$.

For the reaction-diffusion linearization, each Neumann Laplacian eigenmode with eigenvalue $\mu = \lambda_k$ yields the dispersion matrix

$$\mathcal{A}(\mu) = \mathcal{J} - \mu \text{diag}(d_S, d_R) = \begin{pmatrix} \partial_S f_S(\mathbb{K}^*) - \mu d_S & \partial_R f_S(\mathbb{K}^*) \\ \partial_S f_R(\mathbb{K}^*) & \partial_R f_R(\mathbb{K}^*) - \mu d_R \end{pmatrix}.$$

The characteristic polynomial for $\mathcal{A}(\mu)$ is

$$\lambda^2 - \text{tr}(\mathcal{A}(\mu))\lambda + \det(\mathcal{A}(\mu)) = 0,$$

or equivalently,

$$\lambda^2 + \lambda(\mu(d_S + d_R) - \text{tr}(\mathcal{J})) + h(\mu) = 0,$$

where

$$h(\mu) = d_S d_R \mu^2 - (d_S \partial_R f_R(\mathbb{K}^*) + d_R \partial_S f_S(\mathbb{K}^*))\mu + \det(\mathcal{J}).$$

Since $\text{tr}(\mathcal{J}) < 0$ and $\partial_S f_S(\mathbb{K}^*) < 0$, $\partial_R f_R(\mathbb{K}^*) < 0$, we have

$$\mu(d_S + d_R) - \text{tr}(\mathcal{J}) > 0, \quad h(\mu) > 0 \quad \text{for all } \mu > 0.$$

Therefore the Routh–Hurwitz criterion implies $\Re(\lambda(\mu)) < 0$ for all $\mu > 0$, ruling out diffusion-driven destabilization. \square

Remark 3.10 (Block structure for the full base model). Theorem 3.9 is stated for the reduced (S, R) reaction–diffusion subsystem (corresponding to the post-washout $I \equiv 0$ limit), but the same no-Turing conclusion is consistent with the full base model (2).

Fix a Neumann Laplacian eigenvalue $\mu = \lambda_k \geq 0$ and linearize (2) about the homogeneous equilibrium branch with $I^* = 0$, $(S^*, R^*) = \mathbb{K}^*$, and constant stromal pool $P^* + F_a^* = P_T$. After a permutation of variables consistent with the coupling topology (the drug equation is decoupled and the stromal subsystem does not feed back into I), the linearization can be written in block triangular form with diagonal blocks corresponding to I , (P, F_a) , and (S, R) .

The I -block contributes the eigenvalue

$$\lambda_I(\mu) = -\gamma_I - d_I \mu < 0,$$

so the drug field produces no unstable spectrum. The (P, F_a) -block linearizes' to a matrix with spectrum $\{0, -\beta\}$; the zero eigenvalue corresponds to the locally conserved quantity $P + F_a$ and does not generate spatial growth since P and F_a do not diffuse at this level. Finally, the (S, R) -block yields the dispersion matrix $\mathcal{A}(\mu)$ in the proof of Theorem 3.9. Hence the full linearization admits no diffusion-driven (Turing-type) instability under the standing assumptions.

4 Directionality–Damping Principle

4.1 Mechanism statement

Section 3 established a baseline conclusion for the damped hybrid model (2) under homogeneous Neumann boundary conditions: after a single-dose intervention, the drug field I relaxes exponentially, the induced couplings vanish asymptotically, and the remaining dynamics are strongly dissipative. In particular, the post-washout reaction–diffusion core admits no diffusion-driven (Turing-type) bifurcation from homogeneity (Section 3.5).

We now ask how directed transport modifies this baseline, and which structural features determine whether spatial heterogeneity can be generated from a homogeneous equilibrium. Chemotaxis introduces advective fluxes of the form $-\nabla \cdot (\chi_W W \nabla c)$,

which bias migration of a population W toward increasing values of a signal c . Such drift can transiently amplify spatial perturbations, but whether amplification produces a genuine pattern-forming instability is governed by two intertwined features:

- (i) **Directionality of coupling.** In unidirectional (one-way) systems, the populations respond to a signal field but do not regulate it; the feedback loop required for self-reinforcing amplification is therefore absent. In bidirectional (two-way) systems, the signal depends on the populations (e.g. $c = g(S, R)$ or via a produced chemoattractant), closing a feedback loop and modifying the effective transport operator.
- (ii) **Damping/relaxation structure.** Logistic crowding, switching, and signal decay dissipate spatial perturbations and compete against chemotactic focusing. In the present model class, the base kinetics already contain strong damping (logistic competition and drug washout), providing a stringent test for whether directed transport can destabilize homogeneity.

In the unidirectional setting, logistic damping together with signal relaxation implies that the homogeneous equilibrium cannot be destabilized in the Turing sense: one-way sensing is incapable of generating diffusion-driven patterns from homogeneity (Section 4.2). By contrast, bidirectional feedback can destabilize intermediate wavelengths within the well-posed (strongly parabolic) regime (Section 4.3), while exceeding the parabolicity threshold leads to Hadamard instability/aggregation and motivates biological regularization of the chemotactic flux (Section 4.4). The emphasis on generation from homogeneity under closed-loop coupling is consistent with recent tumor microenvironment models in which a chemotactic population both responds to and reinforces the guiding signal (Liu et al. 2025). The numerical experiments in Section 5 illustrate both aspects: robust relaxation in the base and unidirectional regimes, and the restoration of finite-scale patterning only when minimal feedback closes the loop.

4.2 Unidirectional coupling: no diffusion-driven pattern generation

To emphasize transferability beyond the specific tumor–drug–stroma nonlinearities, we consider the unidirectional class (9)–(10), where c is a relaxing signal satisfying $\partial_c \mathcal{Q} < 0$ and the populations (S, R) experience dissipative kinetics. The condition $\partial_c \mathcal{Q} < 0$ ensures that the signal relaxes. The population senses a signal landscape but does not regulate it. In this open-loop setting, the feedback reinforcement required for diffusion-driven bifurcation is absent.

Theorem 4.1 (Unidirectional coupling cannot generate diffusion-driven patterns)
Consider (10) with a unique interior equilibrium $\mathbf{u}^ = (S^*, R^*, c^*)$ and assume $\partial_c \mathcal{Q} < 0$. Let \mathcal{J}_F be the Jacobian of $F = (f_S, f_R)$ at (S^*, R^*) ,*

$$\mathcal{J}_F = \begin{pmatrix} a & b \\ c & d \end{pmatrix}, \quad a = \partial_S f_S(\mathbf{u}^*), \quad b = \partial_R f_S(\mathbf{u}^*), \quad c = \partial_S f_R(\mathbf{u}^*), \quad d = \partial_R f_R(\mathbf{u}^*).$$

Assume the homogeneous kinetics are stable:

$$a + d < 0, \quad ad - bc > 0.$$

Then the homogeneous equilibrium is linearly stable with respect to all non-constant Neumann Laplacian modes provided either

- (i) $dd_S + ad_R < 0$, or
- (ii) $4(ad - bc)d_Sd_R > (dd_S + ad_R)^2$.

In particular, if $d_S = d_R$, stability holds for all modes and no diffusion-driven (Turing-type) bifurcation from homogeneity can occur.

Proof Since the c -equation in (10) is decoupled and satisfies $\partial_c \mathcal{Q} < 0$, its linearization contributes only strictly negative mode-wise eigenvalues. Therefore mode-wise stability is determined by the (S, R) subsystem. For each Neumann Laplacian eigenvalue $\mu = \lambda_k > 0$, the dispersion matrix is

$$\mathcal{A}(\mu) = \mathcal{J}_F - \mu \begin{pmatrix} d_S & 0 \\ 0 & d_R \end{pmatrix}.$$

We have $\text{tr}(\mathcal{A}(\mu)) = (a + d) - \mu(d_S + d_R) < 0$ for all $\mu > 0$. Moreover,

$$\det(\mathcal{A}(\mu)) = (a - \mu d_S)(d - \mu d_R) - bc = d_S d_R \mu^2 - (dd_S + ad_R)\mu + (ad - bc).$$

Let $q(\mu) := \det(\mathcal{A}(\mu))$. Since $d_S d_R > 0$ and $q(0) = ad - bc > 0$, it suffices to ensure $q(\mu) > 0$ for all $\mu \geq 0$. If (i) holds, then the linear term in q is nonnegative and hence $q(\mu) \geq q(0) > 0$ for all $\mu \geq 0$. If (ii) holds, then the discriminant of q is negative and q has no real roots; since $q(0) > 0$ and q is convex, it follows that $q(\mu) > 0$ for all $\mu \geq 0$. In either case, the Routh–Hurwitz criterion yields $\Re \lambda(\mu) < 0$ for all $\mu > 0$.

Finally, if $d_S = d_R = d$, then $\mathcal{A}(\mu) = \mathcal{J}_F - \mu d I$ and the spectrum satisfies $\lambda(\mu) = \lambda(0) - \mu d$ mode-wise. Thus all non-constant modes are strictly more stable than the homogeneous mode, and no diffusion-driven bifurcation can occur. \square

Corollary 4.2 (Application to the unidirectional coupling system with logistic damping) *System (9) is a concrete example of system (10). Therefore the conclusions of Theorem 4.1 apply to (9) with the Jacobian evaluated for the damped kinetics. Specifically, define*

$$\tilde{f}_S(S, R) = \lambda_S S \left(1 - \frac{S+R}{K}\right) + f_S(S, R), \quad \tilde{f}_R(S, R) = \lambda_R R \left(1 - \frac{S+R}{K}\right) + f_R(S, R),$$

and let \mathcal{J}_F in Theorem 4.1 be computed using \tilde{f}_S, \tilde{f}_R in place of f_S, f_R .

Corollary 4.3 (Application to the tumor–drug–stroma unidirectional model) *Consider the unidirectional chemotaxis extension (8), with (I, P, F_a) evolving as in (2) and with the signal c modeled as a decaying open-loop field (i.e. c receives no feedback from (S, R)). Assume the homogeneous equilibrium is linearly stable for the corresponding reduced (S, R) subsystem. Then the homogeneous equilibrium cannot undergo diffusion-driven destabilization induced by the unidirectional chemotactic terms: unidirectional sensing does not generate Turing-type patterns from homogeneity.*

Remark 4.4. Corollary 4.3 is the mechanism-level statement used in the remainder of the paper. The explicit coefficient computations for the concrete model (8) (including the fully expanded dispersion relation) are lengthy and are therefore deferred to Appendix A. The essential point is that in one-way coupling the signal landscape is not reinforced by the migrating populations, so the feedback loop required for diffusion-driven bifurcation is absent.

4.3 Bidirectional feedback: effective mobility and strong parabolicity

We now turn to bidirectional coupling, where the guiding signal depends on the populations and therefore closes a feedback loop. In this setting, the chemotactic drift alters the transport operator itself and can create instability even when the homogeneous kinetics are stable. A key point—both analytically and for interpretation—is that the high-frequency behavior of the linearized problem is governed by an effective mobility matrix. This provides a clean separation between well-posed finite-wavelength (Turing-type) instability and Hadamard instability/aggregation arising from loss of parabolic smoothing.

We work with the bidirectional system (11), and assume it admits an interior equilibrium $\mathbf{u}^* = (S^*, R^*)$ satisfying

$$f_S(S^*, R^*) = 0, \quad f_R(S^*, R^*) = 0.$$

Let \mathcal{J}_F denote the Jacobian of $F = (f_S, f_R)$ at \mathbf{u}^* :

$$\mathcal{J}_F = \begin{pmatrix} a & b \\ c & d \end{pmatrix}, \quad a = \partial_S f_S(\mathbf{u}^*), \quad b = \partial_R f_S(\mathbf{u}^*), \quad c = \partial_S f_R(\mathbf{u}^*), \quad d = \partial_R f_R(\mathbf{u}^*).$$

Linearizing the chemotactic fluxes at \mathbf{u}^* yields the feedback matrix

$$\mathcal{H}(\mathbf{u}^*) = \begin{pmatrix} \chi_S \partial_S g(\mathbf{u}^*) S^* & \chi_S \partial_R g(\mathbf{u}^*) S^* \\ \chi_R \partial_S g(\mathbf{u}^*) R^* & \chi_R \partial_R g(\mathbf{u}^*) R^* \end{pmatrix}.$$

Writing $\tilde{\mathbf{u}} = (S - S^*, R - R^*)^\top$, the linearization takes the form

$$\partial_t \tilde{\mathbf{u}} = (\mathcal{D}_{\text{diff}} - \mathcal{H}(\mathbf{u}^*)) \Delta \tilde{\mathbf{u}} + \mathcal{J}_F \tilde{\mathbf{u}}, \quad \mathcal{D}_{\text{diff}} = \begin{pmatrix} d_S & 0 \\ 0 & d_R \end{pmatrix}.$$

This motivates the definition of the effective mobility matrix

$$M := \mathcal{D}_{\text{diff}} - \mathcal{H}(\mathbf{u}^*) = \begin{pmatrix} d_S - \chi_S \partial_S g(\mathbf{u}^*) S^* & -\chi_S \partial_R g(\mathbf{u}^*) S^* \\ -\chi_R \partial_S g(\mathbf{u}^*) R^* & d_R - \chi_R \partial_R g(\mathbf{u}^*) R^* \end{pmatrix}. \quad (27)$$

For each Neumann Laplacian eigenvalue $\mu = \lambda_k \geq 0$, the mode-wise dispersion matrix is

$$\mathcal{A}(\mu) = \mathcal{J}_F - \mu M, \quad (28)$$

so that the growth rates satisfy $\det(\lambda I - \mathcal{A}(\mu)) = 0$. In particular, the asymptotic behavior as $\mu \rightarrow \infty$ is governed by the principal part $-\mu M$.

To correctly distinguish finite-wavelength pattern selection from high-frequency breakdown, we explicitly isolate the regime in which the linearized diffusion operator is uniformly parabolic.

Assumption 4.5 (Strong parabolicity of the effective mobility). There exists a constant $m_0 > 0$ such that the symmetric part of M satisfies

$$\text{sym}(M) := \frac{M + M^T}{2} \geq m_0 I \quad (\text{as quadratic forms on } \mathbb{R}^2).$$

Equivalently,

$$\xi^T \text{sym}(M) \xi \geq m_0 |\xi|^2 \quad \forall \xi \in \mathbb{R}^2.$$

Remark 4.6 (Sufficient checks in the 2×2 case). Assumption 4.5 is a standard sufficient condition ensuring that the operator associated with M generates a well-posed forward-in-time evolution (high spatial frequencies are damped). Since $\text{sym}(M)$ is symmetric, a convenient sufficient condition is positivity of its trace and determinant:

$$\text{tr}(\text{sym}(M)) > 0, \quad \det(\text{sym}(M)) > 0.$$

When M is symmetric (or approximately symmetric), strong parabolicity reduces to positive definiteness of M , which in the 2×2 case can be checked by

$$\text{tr}(M) > 0, \quad \det(M) > 0.$$

If Assumption 4.5 fails, i.e. $\text{sym}(M)$ has a nonpositive eigenvalue, then high-frequency modes need not be damped. In that case, the dispersion relation associated with (28) may exhibit growth that increases without bound as $\mu \rightarrow \infty$, signaling Hadamard instability/aggregation rather than finite-wavelength Turing pattern selection.

4.4 Bidirectional feedback: stable, finite-band, and ill-posed regimes

We now state the instability classification for bidirectional feedback systems. The distinction hinges on the effective mobility matrix $M = \mathcal{D}_{\text{diff}} - \mathcal{H}(\mathbf{u}^*)$ introduced in (27). When M is strongly parabolic (Assumption 4.5), high-frequency modes are damped and any instability can only occur on a bounded band of intermediate wavelengths (finite-wavelength selection). When strong parabolicity fails, the linearized problem may exhibit Hadamard-type high-frequency amplification, corresponding to aggregation/collapse rather than finite-band Turing pattern selection.

Theorem 4.7 (Bidirectional feedback: stable, Turing-type, and aggregation/ill-posed regimes) Consider the bidirectional system (11) on a bounded smooth domain U

under homogeneous Neumann boundary conditions. Let $\mathbf{u}^* = (S^*, R^*)$ be an interior equilibrium. Let \mathcal{J}_F be the reaction Jacobian at \mathbf{u}^* and let $M = \mathcal{D}_{\text{diff}} - \mathcal{H}(\mathbf{u}^*)$ be the effective mobility matrix, as in (27). For each Neumann Laplacian eigenvalue $\mu = \lambda_k \geq 0$, define the mode-wise dispersion matrix

$$\mathcal{A}(\mu) = \mathcal{J}_F - \mu M,$$

so that growth rates satisfy $\det(\lambda I - \mathcal{A}(\mu)) = 0$. Assume the homogeneous kinetics are stable:

$$\text{tr}(\mathcal{J}_F) < 0, \quad \det(\mathcal{J}_F) > 0. \quad (29)$$

Then the parameter space decomposes into the following regimes:

(i) **Stable (well-posed and mode-wise stable).** If Assumption 4.5 holds and, in addition,

$$\text{tr}(\mathcal{A}(\mu)) < 0 \quad \text{and} \quad \det(\mathcal{A}(\mu)) > 0 \quad \text{for all } \mu \geq 0, \quad (30)$$

then $\Re \lambda(\mu) < 0$ for all modes $\mu \geq 0$. In particular, \mathbf{u}^* is linearly stable and no diffusion-driven instability occurs.

(ii) **Finite-band instability (well-posed with finite-wavelength selection).** Assume Assumption 4.5 holds. If there exists a mode $\mu_* > 0$ such that either

$$\text{tr}(\mathcal{A}(\mu_*)) > 0 \quad \text{or} \quad \det(\mathcal{A}(\mu_*)) < 0, \quad (31)$$

then \mathbf{u}^* is linearly unstable to spatial perturbations. Moreover, due to strong parabolicity, high-frequency modes are damped: there exists $\mu_1 > 0$ such that $\Re \lambda(\mu) < 0$ for all $\mu \geq \mu_1$. Consequently, instability (if present) occurs on a bounded set of intermediate wavelengths, corresponding to finite-wavelength (Turing-type) pattern generation.

(iii) **Aggregation / ill-posedness (loss of parabolic smoothing).** If Assumption 4.5 fails and $\text{sym}(M)$ has a negative eigenvalue, then the principal part of the linearized operator contains a direction of anti-diffusion. In this case the dispersion relation exhibits Hadamard instability in the sense that

$$\sup_{\mu > 0} \Re \lambda(\mu) = +\infty,$$

and the model must be interpreted as an aggregation/collapse limit of the unregularized continuum description (Joseph 1990). This regime should not be interpreted as finite-wavelength Turing pattern selection; rather it indicates that additional physical regularization (e.g. volume filling or flux limitation) is required for biological realism.

Proof sketch The statement follows from the 2×2 dispersion relation associated with $\mathcal{A}(\mu) = \mathcal{J}_F - \mu M$. Under (29), the homogeneous equilibrium is stable at $\mu = 0$. If (30) holds for all $\mu \geq 0$, then the Routh–Hurwitz conditions imply $\Re \lambda(\mu) < 0$ for every mode, giving (i).

Assume next that Assumption 4.5 holds. Then the principal part $-\mu M$ dominates as $\mu \rightarrow \infty$ and yields $\Re \lambda(\mu) \rightarrow -\infty$, so any instability must occur on a bounded interval of μ ; condition (31) guarantees the existence of an unstable mode, giving (ii).

If $\text{sym}(M)$ has a negative eigenvalue, then there exists a direction $\zeta \in \mathbb{R}^2$ such that $\zeta^\top \text{sym}(M) \zeta < 0$. Along the corresponding high-frequency modes, the principal contribution $-\mu M$ produces growth of order $+\mu$, hence $\sup_{\mu > 0} \Re \lambda(\mu) = +\infty$, giving (iii). \square

Remark 4.8 (Interpretation of regimes). Regime (ii) corresponds to finite-wavelength selection: instability occurs only on an intermediate band of modes, while high frequencies remain damped by parabolic smoothing. By contrast, regime (iii) corresponds to Hadamard-type high-frequency amplification, in which the linearized

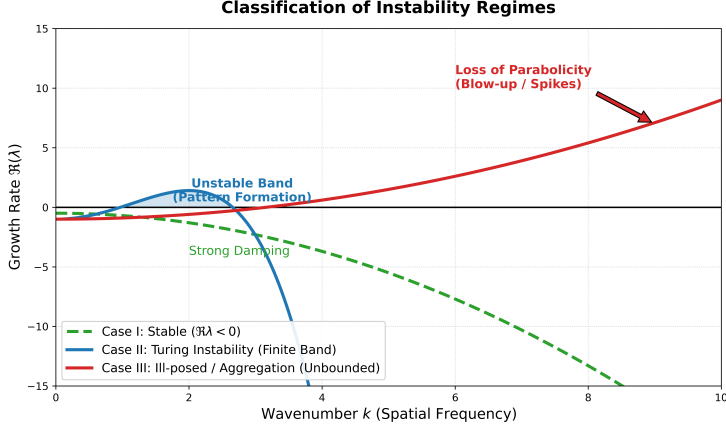


Fig. 5 Classification of stability regimes (Theorem 4.7). Plot of growth rate $\Re(\lambda)$ vs. wavenumber k . **Case I** (green): unconditional stability. **Case II** (blue): well-posed finite-band (Turing-type) instability. **Case III** (red): loss of parabolicity (growth rate diverges), indicating aggregation/ill-posedness.

growth rate can increase without bound as $\mu \rightarrow \infty$. The latter is an aggregation/-collapse signal for the unregularized continuum model and should be interpreted as a prompt to introduce biologically meaningful regularization (e.g. flux limitation) rather than as classical Turing pattern formation. Figure 5 provide representative dispersion curves consistent with Theorem 4.7. The classification result is parallel to the algebraic-spectral separation between different stability properties and bifurcation behaviors (Wang and Yu 2026).

Remark 4.9 (Parabolicity threshold and the need for regularization). A convenient diagnostic for the onset of aggregation/ill-posedness is loss of positivity of the diagonal effective diffusion terms in M . For example, parameter configurations that force

$$d_S - \chi_S \partial_S g(\mathbf{u}^*) S^* < 0 \quad \text{and} \quad d_R - \chi_R \partial_R g(\mathbf{u}^*) R^* = 0,$$

or

$$d_S - \chi_S \partial_S g(\mathbf{u}^*) S^* = 0 \quad \text{and} \quad d_R - \chi_R \partial_R g(\mathbf{u}^*) R^* < 0,$$

push the system toward regime (III) and should be interpreted as aggregation/ill-posedness rather than finite-band Turing patterning.

These conditions have a direct physical interpretation: they quantify when feedback-driven drift becomes comparable to, or exceeds, diffusive smoothing. In partially decoupled limits, the thresholds

$$\chi_S^c = \frac{d_S}{\partial_S g(\mathbf{u}^*) S^*}, \quad \chi_R^c = \frac{d_R}{\partial_R g(\mathbf{u}^*) R^*} \quad (32)$$

mark the point at which taxis-induced focusing can dominate diffusion.

Importantly, exceeding such a threshold in an unregularized continuum model should not automatically be interpreted as biologically smooth “pattern formation”. When feedback becomes strong enough to violate strong parabolicity of the effective mobility matrix $M = \mathcal{D}_{\text{diff}} - \mathcal{H}(\mathbf{u}^*)$ (regime (III) in Theorem 4.7), the linearized dispersion relation can exhibit unbounded high-frequency growth, signaling aggregation/collapse (Hadamard-type instability) rather than finite-wavelength Turing banding. From the standpoint of tissue physics, this corresponds to an “over-attractive” regime where cells (or mass) would concentrate toward delta-like peaks in the absence of additional constraints, which is incompatible with finite cell volume and crowding.

5 Numerical experiments: reproducible evidence for the mechanism

5.1 Numerical scheme and implementation details

This section provides reproducible numerical evidence supporting the mechanism classification developed in Section 4. Our goals are to (i) corroborate relaxation toward homogeneity in the base and unidirectional regimes (Regime I and Regime I'), (ii) demonstrate that sustained finite-wavelength structure is recovered only under bidirectional feedback in a well-posed regime (Regime II), and (iii) illustrate numerical breakdown consistent with the aggregation/ill-posed regime when strong parabolicity is violated (Regime III).

We discretize the coupled system on a uniform Cartesian grid over $U = [0, 1]^2$ with mesh size h and time step Δt . For each diffusing component, we use a semi-implicit Crank–Nicolson update for the diffusion term and treat all remaining terms explicitly (reaction and, when present, taxis). Homogeneous Neumann boundary conditions are imposed by ghost-point reflection, ensuring zero normal flux at the discrete level.

In the baseline hybrid system (2), only (S, R, I) are advanced by the diffusion step. In chemotaxis experiments, the taxis term requires a well-defined signal gradient; accordingly, the signal variable c used in the taxis flux is evolved by a parabolic equation and the same semi-implicit diffusion update is applied to c as well. In the unidirectional experiments we take $\mathcal{Q}(c) = -\rho_c c$, so that $\partial_c \mathcal{Q}(c) = -\rho_c < 0$. Unless otherwise stated, we take $N_x = N_y = 51$ (so $h = 1/(N_x - 1)$) and $\Delta t = 10^{-2}$. We use the time horizon $T_{\text{final}} = 5$ for Regimes I and I'. For the feedback simulations in Regimes II–III we use a longer horizon $T_{\text{final}} = 50$ to allow the feedback-driven structures to develop and saturate.

All simulations are initialized near the relevant homogeneous equilibrium by i.i.d. unbiased perturbations

$$W(x_i, y_j, 0) = W^* + \varepsilon \rho_{i,j}, \quad \rho_{i,j} \sim \mathcal{U}(-1, 1) \text{ i.i.d.},$$

applied to each diffusing component present in the model under study. In particular, for the base system (2) we perturb $W \in \{S, R, I\}$, whereas for chemotaxis extensions we additionally perturb the signal field c . Throughout this section we fix $\varepsilon = 10^{-3}$. Since $I^* = 0$ in the washout equilibrium branch, the perturbation may produce negative

values in the drug field; we enforce the physical constraint by truncating I to be nonnegative after each update. For numerical robustness, we also truncate any negative values of the density variables (S, R) and the signal c to zero after each explicit update.

For the non-diffusing stromal variables (P, F_a) , we enforce the homogeneous pool assumption $P_0(x, y) + F_{a,0}(x, y) \equiv P_T = 1$ by setting $(P, F_a)(x, y, 0) = (P^*, F_a^*) = (1, 0)$.

In Regime II simulations, we employ a flux-saturated (velocity-limited) taxis to prevent non-physical collapse; the explicit form is given in Section 5.4. Baseline parameter values used in the numerical experiments are listed in Table 2. Parameters that are used in a subset of experiments are indicated in the table.

Table 2 Baseline parameter values used in the numerical experiments (units are given in Table 1). Parameters marked “(uni)” are used only in the unidirectional chemotaxis experiments; parameters marked “(fb)” are used only in the feedback experiments.

Parameter	Value	Parameter	Value
d_S	10^{-3}	d_R	10^{-3}
d_I	5	d_c	5×10^{-3}
λ_S	0.5	λ_R	0.5
K	2.0	α	0.1
ξ	0.1	η	0.2
θ	1	β	0.5
γ_I	1	ρ_c	1.6
$\delta(I)$	$\delta_0 \frac{I}{I + K_I}$	$\phi(I)$	$\tanh(\kappa_\phi I)$
δ_0	0.5	K_I	0.5
κ_ϕ	5		
χ_S (uni)	0.5	χ_R (uni)	0.5
χ'_S (fb)	0.5	κ_c (fb)	0.8
α_c (fb)	100	ε	10^{-3}

5.2 Base model: relaxation to homogeneity (Regime I)

We first corroborate the relaxation-to-homogeneity behavior of the base hybrid model under homogeneous Neumann boundary conditions. Starting from unbiased perturbations about the homogeneous equilibrium, diffusion smooths spatial deviations while the damped reaction terms drive trajectories toward the equilibrium branch selected after washout. Figure 6 shows representative snapshots of S at $t = 0, 2.5, 5.0$, illustrating progressive homogenization; by $T = 5.0$ the remaining spatial variation is at the level of numerical microfluctuations.

To quantify the decay of spatial heterogeneity, we track the L^2 -deviation norms

$$E_W(t) := \|W(\cdot, t) - W^*\|_{L^2(U)}, \quad W \in \{S, R, I\}.$$

As shown in Figure 7 (blue solid curve for E_S), the deviation decays approximately exponentially after a short transient period, consistent with dissipativity and with the absence of diffusion-driven pattern generation in Regime I.

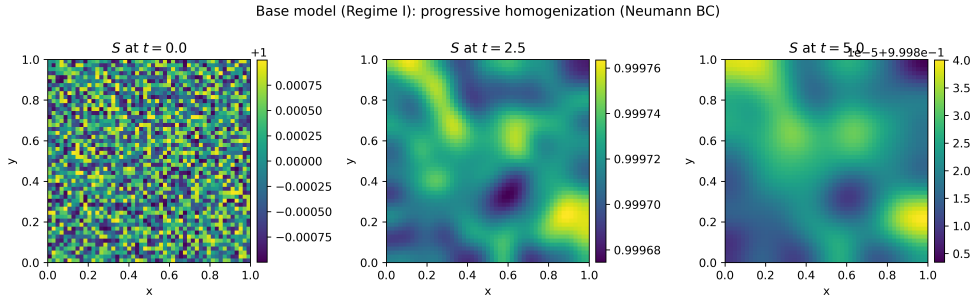


Fig. 6 Base model: progressive homogenization. Spatial snapshots of S at $t = 0, 2.5, 5.0$. Starting from unbiased random perturbations, the field smooths out over time; the colorbar at $t = 5.0$ indicates deviations of order 10^{-4} relative to the mean.

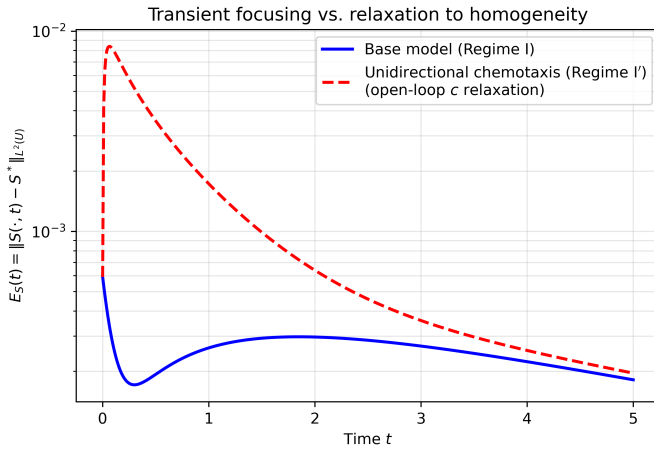


Fig. 7 Quantification of convergence. Evolution of the L^2 -deviation from equilibrium for the base model (blue solid) and the unidirectional chemotaxis model (red dashed). The base model exhibits monotone decay after a transient period. The unidirectional model shows a transient rise followed by decay, consistent with relaxation rather than sustained pattern generation.

5.3 Unidirectional chemotaxis: transient focusing without generation (Regime I')

We next test the “no-generation” prediction for unidirectional coupling (open-loop sensing). In this setting, directed motion can transiently sharpen existing heterogeneity by transporting mass toward prescribed signal maxima, but—in the absence of feedback from (S, R) to the signal—it cannot sustain a diffusion-driven bifurcation from a homogeneous equilibrium. We simulate the unidirectional chemotaxis extension (8) under homogeneous Neumann boundary conditions, using the same initialization protocol as in Section 5.1. Here S and R drift up gradients of the signal field c , while c evolves independently of (S, R) and relaxes in time (we take $\mathcal{Q}(c) = -\rho_c c$).

The resulting dynamics exhibit a characteristic two-phase response. First, a transient increase in the deviation norm $E_S(t) = \|S(\cdot, t) - S^*\|_{L^2(U)}$ may occur as chemotactic drift concentrates mass near local signal maxima. Second, as the signal relaxes and the dissipative reaction terms dominate, the system returns toward the homogeneous equilibrium and $E_S(t)$ decays approximately exponentially. This behavior is shown in Figure 7 (red dashed curve), where the deviation rises briefly and then decreases.

Crucially, no persistent patterned attractor emerges: the transient focusing reflects short-time redistribution along an externally imposed landscape rather than de novo pattern formation from homogeneity. These simulations therefore support the mechanism statement of Section 4.1 and are consistent with the unidirectional stability conclusions of Section 4.2, namely that one-way sensing can amplify perturbations transiently but does not generate sustained diffusion-driven (Turing-type) patterns without closed-loop feedback.

5.4 Bidirectional feedback: finite-band patterns vs aggregation (Regimes II–III)

We now demonstrate the central distinction of the directionality-damping principle: sustained finite-wavelength structure is recovered only when a feedback loop closes the signal landscape. In the unidirectional (open-loop) chemotaxis experiments, the cue evolves independently of (S, R) and relaxes, so chemotaxis may transiently focus mass but cannot generate a persistent patterned attractor from a homogeneous equilibrium. To create the minimal closed-loop mechanism, we introduce an auxiliary chemoattractant field c that is produced by the susceptible population S and decays in time.

We augment the unidirectional system by coupling S to c through a production–diffusion–decay equation, and we include taxis of S along ∇c :

$$\begin{cases} \partial_t S = d_S \Delta S - \chi'_S \nabla \cdot (S \nabla c) + \lambda_S S \left(1 - \frac{S+R}{K}\right) - \alpha S - \delta(I)S + \xi(1 - \phi(I))R, \\ \partial_t c = d_c \Delta c + \kappa_c S - \rho_c c, \end{cases} \quad (33)$$

while keeping (R, I, P, F_a) as in the base system (2). Here κ_c and ρ_c are the production and decay rates of c , and χ'_S is the taxis sensitivity of S to c . This closes the positive feedback loop

$$S \rightarrow c \rightarrow \nabla c \rightarrow \text{drift of } S.$$

For the homogeneous equilibrium of (33), the signal component satisfies $c^* = (\kappa_c/\rho_c) S^*$.

5.4.1 Regime II (well-posed finite-band patterns): flux saturation as a physical regularization

To isolate finite-wavelength selection while preventing non-physical collapse at large focusing strength, we implement a flux-saturated (velocity-limited) taxis in the simulations underlying Figure 8. Concretely, in (33) we replace the linear taxis flux by

$$-\chi'_S \nabla \cdot (S \nabla c) \rightsquigarrow -\nabla \cdot \left(\chi'_S S \frac{\nabla c}{1 + \alpha_c |\nabla c|} \right), \quad (34)$$

with $\alpha_c = 100$ controlling the saturation strength. $\alpha_c = 100$ is chosen to strongly limit drift velocities and prevent grid-scale collapse; qualitative behavior is insensitive within an order of magnitude. This form bounds the drift velocity as $|\nabla c|$ increases, suppressing high-frequency collapse while retaining the intermediate-wavelength destabilization. With this regularization in place, the feedback-augmented system develops persistent finite-wavelength spatial heterogeneity; Figure 8 shows the patterned S field together with the chemoattractant c and a representative cross-section indicating their phase alignment.

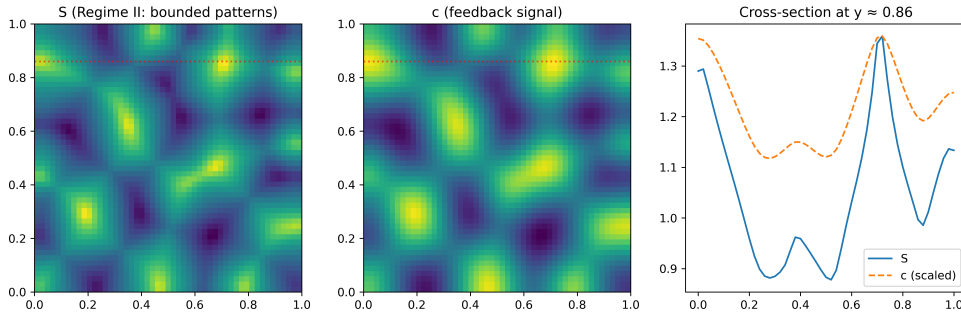


Fig. 8 Restoration of patterning via bidirectional feedback. Left: spatial profile of S showing finite-wavelength structures. Middle: chemoattractant field c generated by S via (33). Right: cross-section at $y = 0.86$ showing phase alignment between S and c .

5.4.2 Regime III (aggregation/ill-posed tendency): removal of saturation

In contrast, when the same feedback system is simulated without flux saturation (i.e., using the linear taxis flux in (33)), the focusing drift can overwhelm diffusive smoothing and rapidly amplify small scales. Numerically, this manifests as overflow/NaN and breakdown rather than a smooth patterned attractor; see Figure 9. Accordingly, we interpret the breakdown as an aggregation tendency that necessitates a regularization mechanism (here: flux limitation), not as classical finite-wavelength pattern formation. In our parameter sweeps (with all other parameters fixed as in Table 2), we observed that the linear taxis sensitivity χ'_S admits a transition: below an $\mathcal{O}(10^{-2})$ level the simulations remain well-behaved and patterns (when present) stay bounded, whereas above this level the unregulated linear flux tends to trigger rapid small-scale amplification and numerical breakdown.

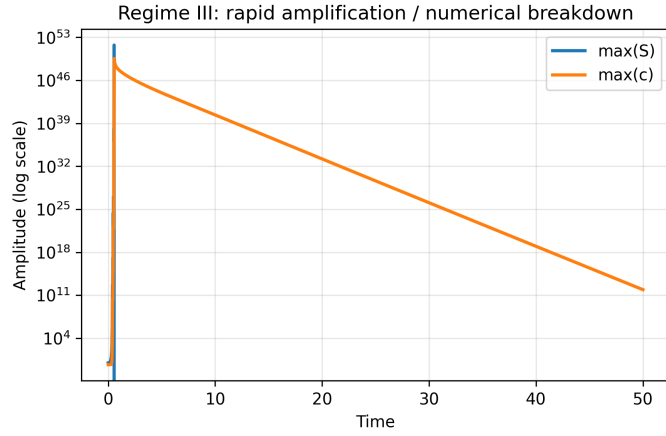


Fig. 9 Numerical breakdown without flux limitation. In the bidirectional feedback setting (33) with the linear taxis flux (no flux limitation), $\max S(t)$ and $\max c(t)$ grow rapidly and the simulation breaks down. This behavior is consistent with aggregation/ill-posedness (Regime III) and signals the need for regularization.

Taken together, the simulations in Regimes I, I', II, and III provide reproducible evidence for the paper's main message: under damping/relaxation, unidirectional coupling relaxes rather than generates persistent patterns, whereas bidirectional feedback can generate finite-wavelength structure in a well-posed regime, with flux regularization separating bounded patterning from aggregation-type breakdown.

6 Discussion

We summarize the main message of this work and place it in the broader context of spatial instability mechanisms in hybrid PDE–ODE models. The proposed framework couples two proliferating tumor phenotypes (S, R) to an exogenously administered

therapeutic agent I (single dose, open loop, no sustained source) and to a stromal switching module (P, A) that is non-diffusing. All PDE components are posed with homogeneous Neumann boundary conditions, representing a closed tissue domain and ensuring compatibility with spatially homogeneous equilibria and with the long-time reduction developed in Section 3. Within this setting, the analysis isolates how the topology of directed transport couplings interacts with damping and signal relaxation to determine whether spatial heterogeneity is generated from homogeneity, or instead decays.

A first structural feature is the open-loop decay of the drug field. Because I satisfies a linear parabolic equation with clearance, it relaxes exponentially after dosing, and therefore all I -dependent couplings in the remaining equations vanish asymptotically through $\delta(I)$ and $\phi(I)$; see Section 3.4. Mathematically, this yields a clean separation between transient drug-mediated effects and the intrinsic long-time behavior selected by the population kinetics. Biologically, it formalizes a limitation of single-dose interventions in an open-loop setting: in the absence of sustained input, drug-mediated modulation alone cannot maintain persistent spatial structure, and any enduring heterogeneity must be supported by an internal generation mechanism.

At the baseline level (no chemotaxis), the model exhibits strong dissipation. Diffusion acts as a spatial smoothing mechanism under Neumann boundary conditions, while logistic competition and switching provide damping in the reaction terms. Consistently, we establish global well-posedness and invariant-region structure, and we show that diffusion-driven (Turing-type) destabilization does not occur for the damped reaction–diffusion core near the post-washout coexistence state; see Section 3.5. This clarifies that the baseline hybrid coupling through (P, A) does not by itself supply a PDE-level pattern generator. In particular, the locally conserved stromal pool in the baseline regime produces a neutral mode in the (P, A) block, but it does not create spatial growth because the stromal variables do not diffuse at this level.

The principal mechanism contribution of the paper is the directionality–damping principle for chemotaxis-augmented extensions (Section 4). Chemotaxis introduces directed drift terms that can amplify spatial perturbations, but whether this amplification constitutes genuine pattern generation depends on two intertwined features: the directionality of coupling (open-loop sensing versus closed-loop feedback) and the damping/relaxation structure (logistic crowding and signal decay). In unidirectional coupling, the populations migrate up a prescribed or independently relaxing signal landscape but do not reinforce it; the autocatalytic loop needed for sustained amplification is therefore absent. Under the decay/damping assumptions encoded in the unidirectional templates, this setting cannot generate diffusion-driven structure from a homogeneous equilibrium, although transient focusing may occur when the signal landscape initially contains heterogeneity; see Section 4.2. In contrast, bidirectional feedback closes the loop by making the guiding landscape depend on the populations, thereby modifying the effective transport operator. This modification produces a sharp classification into three regimes (Section 4.4): a stable regime with decay to homogeneity, a well-posed finite-band regime in which intermediate wavelengths destabilize while high frequencies remain damped, and an aggregation/ill-posed regime

in which strong focusing defeats parabolic smoothing and leads to Hadamard-type high-frequency amplification.

A recurring theme across both the analysis and the numerical experiments is the role of strong parabolicity. In the bidirectional setting, the effective mobility matrix M provides a mathematically precise indicator separating finite-wavelength selection from aggregation tendencies: when $\text{sym}(M)$ remains positive definite, high frequencies are damped and any instability is necessarily confined to a bounded band; when this condition fails, high-frequency modes are no longer controlled and the unregularized continuum description can enter an ill-posed regime. From a modelling perspective, this emphasizes that strong positive feedback and steep taxis responses cannot be pushed arbitrarily far in continuum PDE descriptions without additional physics. Flux saturation and related mechanisms (e.g. volume filling) act as biologically motivated regularizers that restore well-posedness and permit bounded finite-wavelength structure as a stable outcome, as illustrated numerically in Section 5.

Several extensions are natural and remain mathematically tractable within the present framework. Repeated dosing or continuous infusion can be incorporated by adding an input term to the I equation, which would remove the strict $I \rightarrow 0$ long-time reduction while preserving the conceptual separation between open-loop forcing and closed-loop feedback. Allowing small diffusion in the stromal variables (or introducing spatial coupling through tissue remodeling) would remove exact local conservation of $P + A$ and may introduce additional slow modes interacting with the Neumann spectrum. Multiple chemoattractants or phenotype-dependent taxis can be handled within the mobility-matrix perspective, at the expense of higher-dimensional stability conditions. Finally, intrinsic (demographic) variability can be incorporated by adding stochastic terms that preserve nonnegativity in an Itô sense, providing a route to quantify robustness of the regime classification under noise (Abundo 1991; Wang and Yu 2025).

Overall, the results delineate a coherent picture: in a hybrid PDE–ODE setting with a single-dose open-loop drug, persistent spatial heterogeneity requires a genuine generation mechanism, and chemotactic feedback provides such a mechanism precisely when transport remains in a strongly parabolic (or appropriately regularized) regime.

Data Availability:

Data sharing is not applicable to this article as no new data were created or analyzed in this study.

Funding:

All authors of this article have confirmed that this research received no external funding.

Author Contributions

All authors contributed to the study. All authors read and approved the final manuscript.

Ethical statement

The authors declare that the research presented in this manuscript is original and has not been published elsewhere and is not under consideration by another journal. The study was conducted in accordance with ethical principles and guidelines.

Declaration:

All authors declare no competing interests.

Appendix A Unidirectional tumor–drug–stroma chemotaxis: full dispersion relation

This appendix supplies the complete linearization and Neumann-mode dispersion relation for the unidirectional (open-loop) tumor–drug–stroma chemotaxis model used in Section 4.2, thereby justifying Corollary 4.3.

A.1 The unidirectional (open-loop) chemotaxis extension

We consider the following unidirectional extension of the base hybrid model (2). The tumor phenotypes (S, R) undergo Keller–Segel-type drift along the gradient of a signal field $c(x, t)$, while c evolves independently (no feedback from (S, R)). The remaining components (I, P, F_a) evolve as in (2). Concretely,

$$\begin{cases} \partial_t S = d_S \Delta S - \chi_S \nabla \cdot (S \nabla c) + \lambda_S S \left(1 - \frac{S+R}{K}\right) - \alpha S - \delta(I)S + \xi [1 - \phi(I)]R, \\ \partial_t R = d_R \Delta R - \chi_R \nabla \cdot (R \nabla c) + \lambda_R R \left(1 - \frac{S+R}{K}\right) + \alpha S + \eta \phi(I)F_a R - \xi [1 - \phi(I)]R, \\ \partial_t I = d_I \Delta I - \gamma_I I, \\ \partial_t P = -\theta \phi(I)P + \beta [1 - \phi(I)]F_a, \\ \partial_t F_a = \theta \phi(I)P - \beta [1 - \phi(I)]F_a, \\ \partial_t c = d_c \Delta c + \mathcal{Q}(c), \quad \mathcal{Q}'(c) < 0. \end{cases} \quad (\text{A1})$$

Homogeneous Neumann boundary conditions are imposed for the diffusing variables (S, R, I, c) :

$$\partial_n S = \partial_n R = \partial_n I = \partial_n c = 0 \quad \text{on } \partial U \times (0, \infty). \quad (\text{A2})$$

In the baseline hybrid regime (P, F_a) evolves pointwise in x . The signal relaxation condition $\mathcal{Q}'(c) < 0$ encodes strict damping of the open-loop guidance field.

A.2 Homogeneous equilibrium and Jacobian blocks

Let

$$\mathbf{u}^* = (S^*, R^*, I^*, P^*, F_a^*, c^*)$$

be a spatially homogeneous equilibrium of (A1), i.e.

$$\Delta S^* = \Delta R^* = \Delta I^* = \Delta c^* = 0, \quad \mathcal{Q}(c^*) = 0,$$

and the reaction terms vanish at $(S^*, R^*, I^*, P^*, F_a^*)$.

Define, for convenience,

$$\phi^* := \phi(I^*), \quad \delta^* := \delta(I^*), \quad \sigma^* := \xi(1 - \phi^*), \quad \zeta^* := \eta \phi^* F_a^*.$$

The kinetic (S, R) reaction map at fixed (I^*, F_a^*) is

$$F_S(S, R) = \lambda_S S \left(1 - \frac{S+R}{K}\right) - \alpha S - \delta^* S + \sigma^* R, \quad F_R(S, R) = \lambda_R R \left(1 - \frac{S+R}{K}\right) + \alpha S + \zeta^* R - \sigma^* R.$$

Its Jacobian at (S^*, R^*) is

$$\mathcal{J}_{SR} := \begin{pmatrix} a & b \\ c & d \end{pmatrix}, \quad (\text{A3})$$

with the explicit entries

$$\begin{aligned} a &= \partial_S F_S(S^*, R^*) = \lambda_S \left(1 - \frac{2S^* + R^*}{K}\right) - \alpha - \delta^*, \\ b &= \partial_R F_S(S^*, R^*) = -\frac{\lambda_S}{K} S^* + \sigma^*, \\ c &= \partial_S F_R(S^*, R^*) = \alpha - \frac{\lambda_R}{K} R^*, \\ d &= \partial_R F_R(S^*, R^*) = \lambda_R \left(1 - \frac{S^* + 2R^*}{K}\right) + \zeta^* - \sigma^*. \end{aligned} \quad (\text{A4})$$

(The dependence of $\phi(\cdot)$ and $\delta(\cdot)$ on I produces additional forcing terms proportional to the I -perturbation; these appear below and are shown not to affect eigenvalues because the I -equation is open-loop.)

The c -block linearization is scalar and strictly stable:

$$\partial_t \tilde{c} = d_c \Delta \tilde{c} + \mathcal{Q}'(c^*) \tilde{c}, \quad \mathcal{Q}'(c^*) < 0. \quad (\text{A5})$$

The drug block is also strictly stable:

$$\partial_t \tilde{I} = d_I \Delta \tilde{I} - \gamma_I \tilde{I}. \quad (\text{A6})$$

Finally, in the baseline hybrid regime, the stromal switching block is pointwise linear:

$$\partial_t \begin{pmatrix} \tilde{P} \\ \tilde{F}_a \end{pmatrix} = B(I^*) \begin{pmatrix} \tilde{P} \\ \tilde{F}_a \end{pmatrix} + \tilde{I} B_I(I^*) \begin{pmatrix} P^* \\ F_a^* \end{pmatrix}, \quad B(I^*) = \begin{pmatrix} -\theta \phi^* & \beta(1 - \phi^*) \\ \theta \phi^* & -\beta(1 - \phi^*) \end{pmatrix}, \quad (\text{A7})$$

where $B_I(I^*)$ denotes the derivative of $B(I)$ with respect to I at $I = I^*$ (it is proportional to $\phi'(I^*)$). Note that $B(I^*)$ has eigenvalues

$$\lambda_{PA,1} = 0, \quad \lambda_{PA,2} = -(\theta\phi^* + \beta(1 - \phi^*)) \leq 0, \quad (\text{A8})$$

so the (P, F_a) block contributes no positive spectrum. The eigenvalue 0 corresponds to the locally conserved pool $P + F_a$ in the baseline regime.

A.3 Linearization of the chemotaxis terms

Write perturbations

$$S = S^* + \tilde{S}, \quad R = R^* + \tilde{R}, \quad I = I^* + \tilde{I}, \quad P = P^* + \tilde{P}, \quad F_a = F_a^* + \tilde{F}_a, \quad c = c^* + \tilde{c}.$$

Since c^* is spatially constant, $\nabla c^* = 0$. The taxis fluxes linearize to

$$-\chi_S \nabla \cdot (S \nabla c) = -\chi_S \nabla \cdot ((S^* + \tilde{S}) \nabla (c^* + \tilde{c})) = -\chi_S S^* \Delta \tilde{c} + (\text{higher order}),$$

and similarly

$$-\chi_R \nabla \cdot (R \nabla c) = -\chi_R R^* \Delta \tilde{c} + (\text{higher order}).$$

Crucially, the taxis contributes only a forcing from \tilde{c} into the (\tilde{S}, \tilde{R}) equations; it does not modify the (\tilde{S}, \tilde{R}) Jacobian with respect to (\tilde{S}, \tilde{R}) at a homogeneous equilibrium.

A.4 Neumann mode decomposition and the dispersion matrices

Let $\{-\Delta w_k = \mu_k w_k, \partial_n w_k = 0\}_{k \geq 0}$ be the Neumann Laplacian eigenpairs on U , with $\mu_k \geq 0$ and $\{w_k\}$ an orthonormal basis of $L^2(U)$. Expand each perturbation in this basis:

$$\tilde{S} = \sum_k s_k(t) w_k(x), \quad \tilde{R} = \sum_k r_k(t) w_k(x), \quad \tilde{I} = \sum_k i_k(t) w_k(x), \quad \tilde{c} = \sum_k \hat{c}_k(t) w_k(x),$$

and similarly for \tilde{P}, \tilde{F}_a .

For each mode $\mu = \mu_k$, the (\tilde{c}, \tilde{I}) coefficients satisfy the decoupled ODEs

$$\hat{c}'_k = (\mathcal{Q}'(c^*) - d_c \mu) \hat{c}_k, \quad i'_k = -(\gamma_I + d_I \mu) i_k. \quad (\text{A9})$$

Hence

$$\mathcal{Q}'(c^*) - d_c \mu < 0 \quad \forall \mu \geq 0, \quad -(\gamma_I + d_I \mu) < 0 \quad \forall \mu \geq 0,$$

so neither c nor I can contribute unstable eigenvalues.

The (\tilde{S}, \tilde{R}) mode amplitudes satisfy

$$\begin{pmatrix} s_k \\ r_k \end{pmatrix}' = \underbrace{\left(\mathcal{J}_{SR} - \mu \text{diag}(d_S, d_R) \right)}_{=: \mathcal{A}_{SR}(\mu)} \begin{pmatrix} s_k \\ r_k \end{pmatrix} + \mu \begin{pmatrix} \chi_S S^* \\ \chi_R R^* \end{pmatrix} \hat{c}_k + \begin{pmatrix} \Gamma_S \\ \Gamma_R \end{pmatrix} i_k, \quad (\text{A10})$$

where Γ_S, Γ_R are constants determined by derivatives of $\delta(I)$ and $\phi(I)$ at I^* (they are proportional to $\delta'(I^*)$ and $\phi'(I^*)$). The important point is that \hat{c}_k and i_k enter (A10) only as inhomogeneous forcing: the homogeneous part is governed by the 2×2 dispersion matrix

$$\mathcal{A}_{SR}(\mu) = \mathcal{J}_{SR} - \mu \begin{pmatrix} d_S & 0 \\ 0 & d_R \end{pmatrix}. \quad (\text{A11})$$

Likewise, the (\tilde{P}, \tilde{F}_a) block is driven by i_k but has homogeneous dynamics generated by $B(I^*)$ in (A7), with eigenvalues (A8). Therefore, after ordering the mode variables as

$$(\hat{c}_k, i_k, \tilde{p}_k, \tilde{a}_k, s_k, r_k),$$

the full mode-wise linear system is block lower triangular: (\hat{c}_k, i_k) evolve independently, $(\tilde{p}_k, \tilde{a}_k)$ are driven by i_k only, and (s_k, r_k) are driven by (\hat{c}_k, i_k) only. Consequently, the spectrum for each μ is the union of the spectra of the diagonal blocks:

$$\sigma(\mu) = \left\{ \mathcal{Q}'(c^*) - d_c \mu, -(\gamma_I + d_I \mu), 0, -(\theta \phi^* + \beta(1 - \phi^*)), \lambda_{\pm}(\mu) \right\}, \quad (\text{A12})$$

where $\lambda_{\pm}(\mu)$ are the two eigenvalues of $\mathcal{A}_{SR}(\mu)$.

A.5 Explicit trace and determinant of $\mathcal{A}_{SR}(\mu)$

From (A11) and (A3),

$$\text{tr}(\mathcal{A}_{SR}(\mu)) = (a+d) - \mu(d_S + d_R), \quad \det(\mathcal{A}_{SR}(\mu)) = (a - \mu d_S)(d - \mu d_R) - bc. \quad (\text{A13})$$

Equivalently, writing the determinant as a quadratic polynomial in μ ,

$$\det(\mathcal{A}_{SR}(\mu)) = d_S d_R \mu^2 - (d_S d_R + a d_R) \mu + (ad - bc). \quad (\text{A14})$$

Hence the mode-wise characteristic polynomial for the (S, R) block is

$$\lambda^2 - \text{tr}(\mathcal{A}_{SR}(\mu)) \lambda + \det(\mathcal{A}_{SR}(\mu)) = 0, \quad (\text{A15})$$

and the Routh–Hurwitz conditions for $\Re \lambda_{\pm}(\mu) < 0$ are exactly

$$\text{tr}(\mathcal{A}_{SR}(\mu)) < 0, \quad \det(\mathcal{A}_{SR}(\mu)) > 0.$$

A.6 Why the c -block cannot create unstable eigenvalues

The c -equation is autonomous and strictly dissipative at the linear level: by (A9), for every Neumann mode $\mu \geq 0$,

$$\hat{c}'_k = (\mathcal{Q}'(c^*) - d_c \mu) \hat{c}_k, \quad \mathcal{Q}'(c^*) - d_c \mu < 0.$$

Thus the c -block contributes only strictly negative eigenvalues. Moreover, because c receives no feedback from (S, R) in (A1), its block is diagonal in the mode-wise ordering

and cannot be shifted by coupling. The chemotaxis terms appear only as forcing from \hat{c}_k into (s_k, r_k) in (A10), which does not affect the eigenvalues (cf. the block-triangular spectrum union (A12)).

A.7 Completion of Corollary 4.3

Assume the homogeneous equilibrium is kinetically stable in the sense that the (S, R) Jacobian satisfies

$$a + d < 0, \quad ad - bc > 0. \quad (\text{A16})$$

Then $\text{tr}(\mathcal{A}_{SR}(\mu)) < 0$ for all $\mu > 0$ because $\mu(d_S + d_R) > 0$. To ensure stability of every non-constant Neumann mode it suffices to guarantee

$$\det(\mathcal{A}_{SR}(\mu)) > 0 \quad \forall \mu \geq 0,$$

which holds under either of the two standard sufficient conditions (exactly as in Theorem 4.1):

$$d d_S + a d_R < 0, \quad \text{or} \quad 4(ad - bc) d_S d_R > (d d_S + a d_R)^2.$$

Under these conditions, the eigenvalues $\lambda_{\pm}(\mu)$ of the (S, R) dispersion matrix satisfy $\Re \lambda_{\pm}(\mu) < 0$ for all $\mu > 0$.

Finally, the remaining diagonal blocks in (A12) contribute only nonpositive spectrum: the drug eigenvalue is $-(\gamma_I + d_I \mu) < 0$, the signal eigenvalue is $\mathcal{Q}'(c^*) - d_c \mu < 0$, and the stromal block contributes $\{0, -(\theta \phi^* + \beta(1 - \phi^*))\}$ with the zero eigenvalue corresponding to the locally conserved pool in the baseline hybrid regime. Therefore, no diffusion-driven destabilization can arise from unidirectional taxis: open-loop sensing does not generate Turing-type patterns from a homogeneous equilibrium, completing the promised derivation.

A.8 Specialization to the single-dose washout equilibrium

In the single-dose setting emphasized in the main text, the long-time homogeneous equilibrium satisfies $I^* = 0$ (drug washout), hence $\phi^* = \phi(0)$ and $\delta^* = \delta(0) = 0$; in typical choices one has $\phi(0) = 0$, so $\sigma^* = \xi$ and $\zeta^* = 0$. In that case the Jacobian entries (A4) reduce to those of the reduced (S, R) subsystem (25). The dispersion matrix (A11) then matches the unidirectional template in Section 4.2, and the above conditions reduce exactly to the criteria stated in Theorem 4.1.

References

Abundo, M.: A stochastic model for predator-prey systems: basic properties, stability and computer simulation. *Journal of Mathematical Biology* **29**(6), 495–511 (1991) <https://doi.org/10.1007/BF00164048>

Amann, H.: Linear and Quasilinear Parabolic Problems. Birkhäuser Basel, Basel (1995). <https://doi.org/10.1007/978-3-0348-9221-6>

Arumugam, G., Tyagi, J.: Keller-segel chemotaxis models: a review. *Acta Applicandae Mathematicae* **171**(1), 6 (2021) <https://doi.org/10.1007/s10440-020-00374-2>

Budrene, E.O., Berg, H.C.: Complex patterns formed by motile cells of *Escherichia coli*. *Nature* **349**(6310), 630–633 (1991) <https://doi.org/10.1038/349630a0>

Budrene, E.O., Berg, H.C.: Dynamics of formation of symmetrical patterns by chemotactic bacteria. *Nature* **376**(6535), 49–53 (1995) <https://doi.org/10.1038/376049a0>

Belik, V., Geisel, T., Brockmann, D.: Natural human mobility patterns and spatial spread of infectious diseases. *Physical Review X* **1**(1), 011001 (2011) <https://doi.org/10.1103/PhysRevX.1.011001>

Bubba, F., Pouchol, C., Ferrand, N., Vidal, G., Almeida, L., Perthame, B., Sabbah, M.: A chemotaxis-based explanation of spheroid formation in 3D cultures of breast cancer cells. *Journal of Theoretical Biology* **479**, 73–80 (2019) <https://doi.org/10.1016/j.jtbi.2019.07.002>

Cornish-Bowden, A.: One hundred years of Michaelis–Menten kinetics. *Perspectives in Science* **4**, 3–9 (2015) <https://doi.org/10.1016/j.pisc.2014.12.002>

Chen, Y., Buceta, J.: A non-linear analysis of Turing pattern formation. *PLOS ONE* **14**(8), 0220994 (2019) <https://doi.org/10.1371/journal.pone.0220994>

Cherniha, R., Davydovych, V.: Nonlinear Reaction-diffusion Systems. Lecture Notes in Mathematics, vol. 2196. Springer, Cham (2017). <https://doi.org/10.1007/978-3-319-65467-6>

Cross, M.C., Hohenberg, P.C.: Pattern formation outside of equilibrium. *Reviews of Modern Physics* **65**(3), 851–1112 (1993) <https://doi.org/10.1103/RevModPhys.65.851>

Chertock, A., Kurganov, A., Wang, X., Wu, Y.: On a chemotaxis model with saturated chemotactic flux. *Kinetic & Related Models* **5**(1), 51–95 (2012) <https://doi.org/10.3934/krm.2012.5.51>

Colizza, V., Pastor-Satorras, R., Vespignani, A.: Reaction–diffusion processes and metapopulation models in heterogeneous networks. *Nature Physics* **3**(4), 276–282 (2007) <https://doi.org/10.1038/nphys560>

Choi, Y., Wang, Z.: Prevention of blow-up by fast diffusion in chemotaxis. *Journal of Mathematical Analysis and Applications* **362**(2), 553–564 (2010) <https://doi.org/10.1016/j.jmaa.2009.08.012>

David, O.I., Mmaduabuchi, I.G., Ugonna, U.K., Akintayo, E.A., Gyang, M., Quadri,

O.N., Rono, C., Ralph-Okhiria, O.H., Praise, O.: The role of the tumor microenvironment in cancer progression and metastasis. *Journal of Cancer and Tumor International* **15**(2), 126–154 (2025) <https://doi.org/10.9734/jcti/2025/v15i2297>

Dolnik, M., Zhabotinsky, A.M., Epstein, I.R.: Resonant suppression of Turing patterns by periodic illumination. *Physical Review E* **63**(2), 026101 (2001) <https://doi.org/10.1103/PhysRevE.63.026101>

Esfahani, P., Levine, H., Mukherjee, M., Sun, B.: Three-dimensional cancer cell migration directed by dual mechanochemical guidance. *Physical Review Research* **4**(2), 022007 (2022) <https://doi.org/10.1103/PhysRevResearch.4.L022007>

Evans, L.C.: *Partial Differential Equations*, Second edition edn. Graduate studies in mathematics, vol. 19. American Mathematical Society, Providence, Rhode Island (2022)

Goldbeter, A.: *Biochemical Oscillations and Cellular Rhythms: the Molecular Bases of Periodic and Chaotic Behaviour*, transferred to digital printing edn. Cambridge University Press, Cambridge (2004)

Haddad, W.M., Chellaboina, V.: *Nonlinear Dynamical Systems and Control: a Lyapunov-based Approach*. Princeton University Press, Princeton (2011)

Henry, D.: *Geometric Theory of Semilinear Parabolic Equations*. Lecture Notes in Mathematics, vol. 840. Springer, Berlin, Heidelberg (1981). <https://doi.org/10.1007/BFb0089647>

Horstmann, D.: From 1970 until present: the keller-segel model in chemotaxis and its consequences (2003)

Höfer, T., Sherratt, J.A., Maini, P.K.: *Dictyostelium discoideum* : cellular self-organization in an excitable biological medium. *Proceedings of the Royal Society of London. Series B: Biological Sciences* **259**(1356), 249–257 (1995) <https://doi.org/10.1098/rspb.1995.0037>

Horstmann, D., Winkler, M.: Boundedness vs. blow-up in a chemotaxis system. *Journal of Differential Equations* **215**(1), 52–107 (2005) <https://doi.org/10.1016/j.jde.2004.10.022>

Jäger, W., Luckhaus, S.: On explosions of solutions to a system of partial differential equations modelling chemotaxis. *Transactions of the American Mathematical Society* **329**(2), 819–824 (1992) <https://doi.org/10.1090/S0002-9947-1992-1046835-6>

Jin, T., Li, Y., Yan, J.: Critical blow-up exponent in a Keller-Segel system with flux limitation and indirect signal production. *Journal of Mathematical Analysis and Applications* **554**(1), 129916 (2026) <https://doi.org/10.1016/j.jmaa.2025.129916>

Joseph, D.D.: Hadamard instability and frozen coefficients. In: *Fluid Dynamics of Viscoelastic Liquids* vol. 84, pp. 69–100. Springer, New York, NY (1990). https://doi.org/10.1007/978-1-4612-4462-2_4

Kondo, S., Miura, T.: Reaction-diffusion model as a framework for understanding biological pattern formation. *Science* **329**(5999), 1616–1620 (2010) <https://doi.org/10.1126/science.1179047>

Kowalczyk, R.: Preventing blow-up in a chemotaxis model. *Journal of Mathematical Analysis and Applications* **305**(2), 566–588 (2005) <https://doi.org/10.1016/j.jmaa.2004.12.009>

Keller, E.F., Segel, L.A.: Initiation of slime mold aggregation viewed as an instability. *Journal of Theoretical Biology* **26**(3), 399–415 (1970) [https://doi.org/10.1016/0022-5193\(70\)90092-5](https://doi.org/10.1016/0022-5193(70)90092-5)

Keller, E.F., Segel, L.A.: Model for chemotaxis. *Journal of Theoretical Biology* **30**(2), 225–234 (1971) [https://doi.org/10.1016/0022-5193\(71\)90050-6](https://doi.org/10.1016/0022-5193(71)90050-6)

LaSalle, J.: Some extensions of liapunov's second method. *IRE Transactions on Circuit Theory* **7**(4), 520–527 (1960) <https://doi.org/10.1109/TCT.1960.1086720>

Lushnikov, P.M., Chen, N., Alber, M.: Macroscopic dynamics of biological cells interacting via chemotaxis and direct contact. *Physical Review E* **78**(6), 061904 (2008) <https://doi.org/10.1103/PhysRevE.78.061904>

Li, S., Muneoka, K.: Cell migration and chick limb development: chemotactic action of FGF-4 and the AER. *Developmental Biology* **211**(2), 335–347 (1999) <https://doi.org/10.1006/dbio.1999.9317>

Ladyženskaja, O.A., Solonnikov, V.A., Ural'ceva, N.N.: *Linear and Quasi-linear Equations of Parabolic Type*. American Mathematical Society, Providence, R.I (1968)

Liu, Z., Wang, L.S., Yu, J., Zhang, J., Martel, E., Li, S.: Bidirectional endothelial feedback drives turing-vascular patterning and drug-resistance niches: a hybrid PDE-agent-based study. *Bioengineering* **12**(10), 1097 (2025) <https://doi.org/10.3390/bioengineering12101097>

Liang, Y., Wang, L.S., Yu, J., Liu, Z.: Global well-posedness and stability of nonlocal damage-structured lineage model with feedback and dedifferentiation. *Mathematics* **13**(22), 3583 (2025) <https://doi.org/10.3390/math13223583>

Martiel, J., Goldbeter, A.: A model based on receptor desensitization for cyclic AMP signaling in dictyostelium cells. *Biophysical Journal* **52**(5), 807–828 (1987) [https://doi.org/10.1016/S0006-3495\(87\)83275-7](https://doi.org/10.1016/S0006-3495(87)83275-7)

Meads, M.B., Gatenby, R.A., Dalton, W.S.: Environment-mediated drug resistance: a major contributor to minimal residual disease. *Nature Reviews Cancer* **9**(9), 665–674 (2009) <https://doi.org/10.1038/nrc2714>

Milne, A., Marusyk, A., Maini, P.K., Anderson, A.R.A., Picco, N.: The role of environmentally mediated drug resistance in facilitating the spatial distribution of residual disease. *Communications Biology* **8**(1), 1189 (2025) <https://doi.org/10.1038/s42003-025-08585-9>

Monk, P.B., Othmer, H.G.: Cyclic AMP oscillations in suspensions of *Dictyostelium discoideum*. *Philosophical Transactions of the Royal Society of London. B, Biological Sciences* **323**(1215), 185–224 (1989) <https://doi.org/10.1098/rstb.1989.0005>

Murray, J.D. (ed.): *Mathematical Biology: I. An Introduction. Interdisciplinary Applied Mathematics*, vol. 17. Springer, New York, NY (2002). <https://doi.org/10.1007/b98868>

Murray, J.D. (ed.): *Mathematical Biology: II: Spatial Models and Biomedical Applications. Interdisciplinary Applied Mathematics*, vol. 18. Springer, New York, NY (2003). <https://doi.org/10.1007/b98869>

Najafi, M., Goradel, N.H., Farhood, B., Salehi, E., Solhjoo, S., Toolee, H., Kharazinejad, E., Mortezaee, K.: Tumor microenvironment: Interactions and therapy. *Journal of Cellular Physiology* **234**(5), 5700–5721 (2019) <https://doi.org/10.1002/jcp.27425>

Oudin, M.J., Weaver, V.M.: Physical and chemical gradients in the tumor microenvironment regulate tumor cell invasion, migration, and metastasis. *Cold Spring Harbor Symposia on Quantitative Biology* **81**, 189–205 (2016) <https://doi.org/10.1101/sqb.2016.81.030817>

Puliafito, A., De Simone, A., Seano, G., Gagliardi, P.A., Di Blasio, L., Chianale, F., Gamba, A., Primo, L., Celani, A.: Three-dimensional chemotaxis-driven aggregation of tumor cells. *Scientific Reports* **5**(1), 15205 (2015) <https://doi.org/10.1038/srep15205>

Painter, K.J., Maini, P.K., Othmer, H.G.: Stripe formation in juvenile *Pomacanthus* explained by a generalized Turing mechanism with chemotaxis. *Proceedings of the National Academy of Sciences* **96**(10), 5549–5554 (1999) <https://doi.org/10.1073/pnas.96.10.5549>

Painter, K.J., Maini, P.K., Othmer, H.G.: A chemotactic model for the advance and retreat of the primitive streak in avian development. *Bulletin of Mathematical Biology* **62**(3), 501–525 (2000) <https://doi.org/10.1006/bulm.1999.0166>

Rothe, F.: *Global Solutions of Reaction-diffusion Systems. Lecture Notes in Mathematics*, vol. 1072. Springer, Berlin, Heidelberg (1984). <https://doi.org/10.1007/BFb0099278>

Sahai, E., Astsaturov, I., Cukierman, E., DeNardo, D.G., Egeblad, M., Evans, R.M.: A framework for advancing our understanding of cancer-associated fibroblasts. *Nature Reviews Cancer* **20**(3), 174–186 (2020) <https://doi.org/10.1038/s41568-019-0238-1>

Smoller, J.: Shock Waves and Reaction—diffusion equations. *Grundlehren der mathematischen Wissenschaften*, vol. 258. Springer, New York, NY (1994). <https://doi.org/10.1007/978-1-4612-0873-0>

Spiro, P.A., Parkinson, J.S., Othmer, H.G.: A model of excitation and adaptation in bacterial chemotaxis. *Proceedings of the National Academy of Sciences* **94**(14), 7263–7268 (1997) <https://doi.org/10.1073/pnas.94.14.7263>

Turing, A.M.: The chemical basis of morphogenesis. *Philosophical Transactions of the Royal Society of London. Series B, Biological Sciences* **237**(641), 37–72 (1952) <https://doi.org/10.1098/rstb.1952.0012>

Wang, Z.A.: On chemotaxis models with cell population interactions. *Mathematical Modelling of Natural Phenomena* **5**(3), 173–190 (2010) <https://doi.org/10.1051/mmnp/20105311>

Wells, D.K., Chuang, Y., Knapp, L.M., Brockmann, D., Kath, W.L., Leonard, J.N.: Spatial and functional heterogeneities shape collective behavior of tumor-immune networks. *PLOS Computational Biology* **11**(4), 1004181 (2015) <https://doi.org/10.1371/journal.pcbi.1004181>

Watts, T.L., Cui, R., Szaniszlo, P., Resto, V.A., Powell, D.W., Pinchuk, I.V.: PDGF-AA mediates mesenchymal stromal cell chemotaxis to the head and neck squamous cell carcinoma tumor microenvironment. *Journal of Translational Medicine* **14**(1), 337 (2016) <https://doi.org/10.1186/s12967-016-1091-6>

Wrzosek, D.: Volume filling effect in modelling chemotaxis. *Mathematical Modelling of Natural Phenomena* **5**(1), 123–147 (2010) <https://doi.org/10.1051/mmnp/20105106>

Wang, L.S., Yu, J.: Analysis framework for stochastic predator–prey model with demographic noise. *Results in Applied Mathematics* **27**, 100621 (2025) <https://doi.org/10.1016/j.rinam.2025.100621>

Wang, L.S., Yu, J.: Algebraic–spectral thresholds and discrete–continuous stability transfer in Leslie–Gower systems. *Electronic Research Archive* **34**(1), 251–290 (2026) <https://doi.org/10.3934/era.2026013>

Wang, L.S., Yu, J., Li, S., Liu, Z.: Analysis and mean-field limit of a hybrid PDE–ABM modeling angiogenesis-regulated resistance evolution. *Mathematics* **13**(17), 2898 (2025) <https://doi.org/10.3390/math13172898>

Yang, X., Dormann, D., Münsterberg, A.E., Weijer, C.J.: Cell movement patterns

during gastrulation in the chick are controlled by positive and negative chemotaxis mediated by FGF4 and FGF8. *Developmental Cell* **3**(3), 425–437 (2002) [https://doi.org/10.1016/S1534-5807\(02\)00256-3](https://doi.org/10.1016/S1534-5807(02)00256-3)

Yuan, Y.: Spatial heterogeneity in the tumor microenvironment. *Cold Spring Harbor Perspectives in Medicine* **6**(8), 026583 (2016) <https://doi.org/10.1101/cshperspect.a026583>

Zhang, X., Ma, H., Gao, Y., Liang, Y., Du, Y., Hao, S., Ni, T.: The tumor microenvironment: signal transduction. *Biomolecules* **14**(4), 438 (2024) <https://doi.org/10.3390/biom14040438>